THEORETICAL AND EXPERIMENTAL APPROACHES IN SCIENTIFIC STUDIES

Editor:

Assoc. Prof. Dr. Ahmet TURŞUCU

Assoc. Prof. Dr. Asaf Tolga ÜLGEN

yaz
yayınları

THEORETICAL AND EXPERIMENTAL APPROACHES IN SCIENTIFIC STUDIES

Editors

Assoc. Prof. Dr. Ahmet TURŞUCU

Assoc. Prof. Dr. Asaf Tolga ÜLGEN

yaz yayınları

2024

yaz yayınları

THEORETICAL AND EXPERIMENTAL APPROACHES IN SCIENTIFIC STUDIES

Editor: Assoc. Prof. Dr. Ahmet TURŞUCU

ORCID NO: 0000-0002-4963-697X

Editor: Assoc. Prof. Dr. Asaf Tolga ÜLGEN

ORCID NO: 0000-0002-7112-5607

E_ISBN 978-625-6104-82-2

Aralık 2024 – Afyonkarahisar

Dizgi/Mizanpaj: YAZ Yayınları

Kapak Tasarım: YAZ Yayınları

YAZ Yayınları. Yayıncı Sertifika No: 73086

M.İhtisas OSB Mah. 4A Cad. No:3/3
İscehisar/AFYONKARAHİSAR

www.yazyayinlari.com

yazyayinlari@gmail.com

info@yazyayinlari.com

CONTENTS

MOLD FLUXES FOR CONTINUOUS CASTING PROCESSES

Mustafa SEYREK[1]

1. INTRODUCTION

In recent years, the continuous method has emerged as the predominant technique for steel production, making up approximately 90% of the global steel supply (Brandaleze, Di Gresia, Santini, Martin & Benavidez, 2012). This approach is preferred because of its exceptional efficiency, productivity, and product quality (Wolf, 2003). The continuous casting process comprises various essential elements, including a pouring ladle, a pouring basin, a submerged entry nozzle (SEN), a water-cooled mold, and a cooling system, as illustrated in Figure 1.

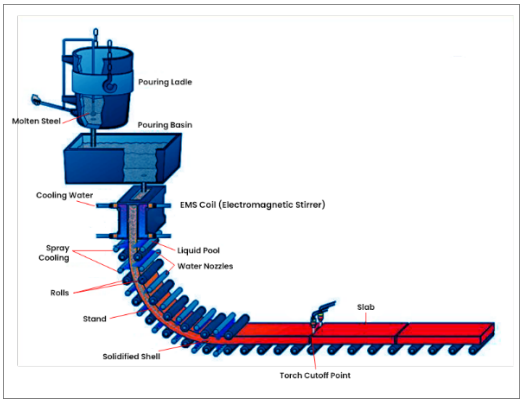

Figure1. Continuous caster (Samrudhi Eng., 2022)

[1] Assist. Prof. Dr., Hitit University, Vocational School of Technical Sciences, mustafaseyrek@hitit.edu.tr, 0000-0001-5386-4804

Figure 1 illustrates the initial step of the continuous casting process, which involves transferring the molten steel from the pouring ladle to the pouring basin and subsequently into the copper mold using the SEN (Brandaleze, et al. 2012). The SEN (Submerged Entry Nozzle) has a vital function in controlling the movement of steel and ensuring a consistent surface level in the mold. In order to facilitate this procedure, mold flux is administered onto the molten steel within the mold. The flux is consistently refilled to guarantee that the surface of the metal remains completely covered (Bothma, 2006). The process of solidification initiates within the copper mold that is cooled by water, and it progresses further through the secondary cooling system, ultimately yielding the final steel product. This product is commonly found in the shape of slabs or billets (Brandaleze, et al. 2012).

Mold fluxes, which are essentially artificial slags, comprise a blend of several oxides including SiO_2, Al_2O_3, CaO, Na_2O, as well as carbon and fluorine (Arefpour, Monshi, Khayamian & Saidi, 2012). The primary roles of these functions are to facilitate lubrication of the steel strand and regulate the transfer of heat within the mold (Kromhout, 2011).

During the casting process, the addition of mold flux to the molten steel goes through a series of changes: it first forms a sinter layer, then transitions into a semi-solid state, and ultimately transforms into a liquid slag layer (as depicted in Figure 4). The liquid slag facilitates lubrication by permeating the gap between the steel strand and the oscillating mold. When the cool mold is first touched, a thin

layer of glassy slag film is created, which might partially crystallise as time passes. The thickness and characteristics of this compact slag layer control the thermal conduction within the mold. The liquid slag provides temporary lubrication, while the solid layer primarily facilitates heat exchange between the steel shell and the mold (Mills, Fox, Thackray & Li, 2004). To attain superior steel quality, it is crucial to ensure appropriate lubrication and controlled horizontal heat transfer. However, the overall mold heat transfer is regulated to avoid any casting flaws (Bothma, 2006).

The continuous steel casting process is complex and often suffers from surface flaws that occur during the early solidification of the steel. These defects are typically linked to the efficacy of the mould flux and may include longitudinal cracking, star cracks, oscillation marks, breakouts, and chemical interactions between the molten steel and air. The aforementioned issues provide significant operational challenges in the continuous casting of steel (Elahipanah, 2012).

2. MOLD FLUXES

Continuous casting mold fluxesare artificial slags that are introduced onto the surface of the molten pool. Their purpose is to facilitate the movement of the steel strand as it passes through the copper mold, which is cooled by water. The surface integrity of the steel product is highly contingent on the efficacy of the mold flux during the process. Mold fluxes exert significant influence over various aspects of the casting process and ultimate quality,

including production rate, surface quality, cleanliness, and defect occurrence (Yan, Yang, Chen, Barati, McLean, 2016; Assia and Adel, 2012). The primary functions of mold fluxes are outlined in Section 2.2.

2.1. Historical Background of Mold Fluxes

Continuous casting is a prominent and widely used method for steel production (Yan et al.,2016; Assia & Adel 2012; Cruz, Chavez, Romero, Palacios & Arredondo, 2017). Currently, the global production of steel has significantly increased to 1.8 million tonnes annually, with almost 95% of this amount being produced using continuous casting (Saraswat, Fox, Mills, Lee & Deo, 2004). The successful outcome of this process is largely attributed to the efficient utilisation of mold fluxes (Wei, Yang, Feng, Sommerville, & McLean, 2006).

Mold fluxes were first utilised in 1958 in Belgium for ingot casting, and by 1963, they were incorporated into continuous casting techniques. The initial iterations of these fluxes were obtained from fly ash, a residual product of power generation that is abundant in Al_2O_3 and SiO_2, and also contains residual carbon and small amounts of CaO and FeO (Mills, 2017).

In the past, casting processes commonly involved the use of oil and carbonaceous substances. However, mold fluxes became more popular due to their ability to enhance thermal insulation of the steel's surface and to extract impurities from the steel. In addition, the liquefied residue produced by these fluxes created a safeguarding layer on top of the molten steel, preventing it from undergoing oxidation (Mills, 2017).

During the last sixty years, there has been significant progress in the utilisation and comprehension of mold fluxes in the process of steel casting. With the advancement of power station efficiency, the amount of carbon in fly ash decreased significantly. This led to a change in using synthetic mold fluxes to improve quality control. However, due to their economical nature, fly ash-based mold fluxes continue to be widely utilised, especially in ingot casting (Mills, 2017; Sighinolfi & Paganelli, 2011).

2.2. Roles of Mold Flux

Mold fluxes have a crucial and essential function in the field of steel casting, as they are primarily responsible for:

- Providing thermal insulation
- Preserving the steel meniscus from oxidation
- Facilitating strand lubrication
- Managing heat transfer
- Capturing impurities (Mills et al., 2004)

Among these, the lubrication of the steel strand and the regulation of heat transfer within the mold stand out as the most crucial functions. Their direct influence on the surface quality of the steel and the overall stability of the process is the reason for their significance (Kromhout, 2011).

2.2.1. Thermal insulation

The primary role of mold fluxes in the continuous casting process is to guarantee sufficient thermal

insulation. The insulation is crucial in order to prevent premature solidification of the liquid steel. Ensuring efficient insulation at the meniscus region is crucial in minimising the severity of oscillation marks and minimising the occurrence of pinholes. Figure 2 demonstrates that reducing the length of the meniscus hook can effectively decrease both the occurrence of pinholes and the depth of oscillation marks (Mills et al., 2004)

Inadequate thermal insulation might result in operating difficulties, including noticeable oscillation marks and breakouts (Brandaleze, et al. 2012). In general, enhanced thermal insulation can be attained through various methods:

- Minimising the dimensions of the mold flux particles
- Increasing the thickness of the flux coating layer
- Incorporating exothermic components, such as combinations of calcium and silicon

In addition, mold fluxes containing extruded granules provide superior thermal insulation in comparison to those containing spherical granules (Mills et al., 2004). In order to enhance the insulating qualities, it is customary to incorporate graphite into the mold fluxes at a concentration ranging from 3% to 6% (Cruz et al., 2007).

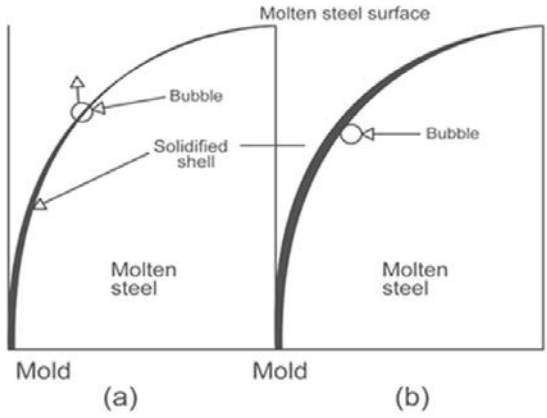

Figure 2 The diagram shows how gas bubbles move depending on the length of the meniscus: (a) it depicts the ascent of a gas bubble unimpeded by a short meniscus; and (b) it demonstrates how a gas bubble becomes trapped by a lengthy meniscus (Mills et al., 2004).

2.2.2. Protecting the Steel Meniscus from Oxidative Reactions

During continuous casting, many layers are formed on the surface of the liquid steel by the mold flux, as shown in Figure 3. The layers serve as a protective barrier, shielding the liquid steel meniscus from oxidation and entrapping gases like nitrogen. To prevent oxidation, it is crucial to maintain a continuous and intact layer of molten slag within the mold (Brandaleze et al., 2012; Kromhout, 2011).

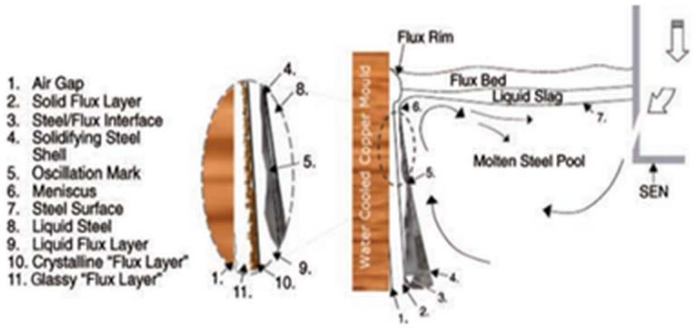

Figure 3 The diagram illustrates the several levels created by mold flux within the mold (Saraswat, Fox, K. Mills, Lee & Deo, 2004)

2.2.3. Lubrication of the Strand

The presence of mold flux between the mold wall and the solidified shell is crucial for lubrication. Effective lubrication provided by the slag is essential to prevent problems such as star cracking. If the flux fully crystallises at the lower area of the mold, it can result in a substantial decrease in lubrication (Mills et al., 2004).

The lubricating efficacy of the mold flux is impacted by various parameters, such as its viscosity and solidification temperature. Improved lubrication is often accomplished by using a flux with a reduced viscosity and/or melting temperature (Wei et al., 2006).Moreover, the effectiveness of the liquid slag as a lubricant is influenced by critical process factors including superheat temperature, nozzle configuration, and casting speed. The presence of any irregularities in the slag layer can increase the likelihood of sticker breakouts (Brandaleze et al., 2012).

2.2.4. Management of Heat Transfer

The heat transfer within the mold can be classified into two main categories: horizontal and vertical. The horizontal heat transfer plays a crucial function in impacting surface imperfections in the end steel product. On the other hand, it is essential to efficiently control the upward movement of heat in order to minimise operational issues such as pinholes and oscillation marks (Brandaleze et al., 2012). Figure 4 illustrates a schematic depiction of the two paths of heat transfer in the mold.

The regulation of heat transfer in the mold is primarily contingent on the separation between the steel shell and the mold wall. This disparity can impede the regulation of thermal conduction. To reduce this disparity, it is necessary to maintain a consistent and ample supply of liquid flux. Therefore, it is crucial to carefully choose a mold flux that has melting qualities that match these requirements, and it should be customised to meet the requirements of various steel grades (Sighinolfi & Paganelli, 2011).

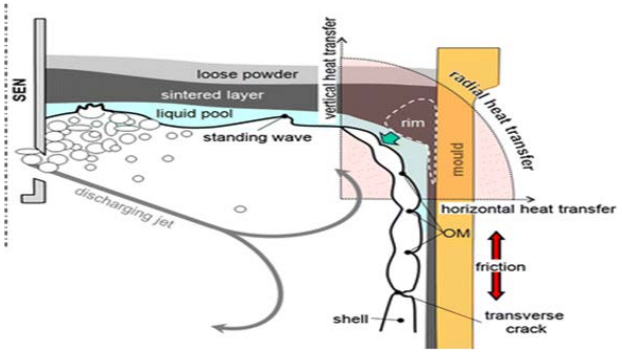

Figure 4. Illustration representing the vertical and horizontal movement of heat within the mold (Mills, 2017).

2.2.5. Impurity Entrapment

The flux capacity to trap inclusions at the interface between liquid slag and metal is vital, as it greatly contributes to the prevention of defects including slivers, blisters and pinholes (Mills, 2003). A liquid slag layer on the meniscus is highly efficient in capturing inclusions, particularly those composed of alumina (Al_2O_3). The creation of Al_2O_3 is a result of a chemical process taking place at the contact.

$$4\,[Al] + (3\,SiO_2)_{(slag)} \rightarrow 2\,(Al_2O_3) + 3\,[Si] \qquad (1)$$

An elevation in the alumina concentration can result in an escalation in slag thickness, which in turn modifies the way the slag film solidifies and therefore affects the overall smoothness of the steel surface (Kromhout, 2011).

To improve the capture of inclusions, one can utilise fluxes that have a high ratio of (CaO/SiO_2) or are abundant in Li_2O, CaF_2, and Na_2O, while being low in TiO_2 and Al_2O_3. Additionally, it has been noted that larger inclusions exhibit greater mobility towards the metal-slag interface, while smaller particles necessitate a longer duration to undergo a similar transformation (Brandaleze et al., 2012).

2.3. Composition of Mold Fluxes

The selection of mold fluxes is typically based on their chemical composition and physical properties, including melting temperature, basicity (expressed as the CaO/SiO_2 ratio), viscosity, free carbon content, and solidification temperature. Nevertheless, these qualities are not directly dictated by the basic minerals themselves (Kromhout,2013). The formulation of mold fluxes is

obtained from a meticulously chosen assortment of basic components, which eventually determine its chemical composition. The typical raw materials utilised consist of fluorite, wollastonite, feldspar, natrite and sources of unbound carbon like coke particles (Kromhout, 2011). Table 1 presents a standard composition profile of mold fluxes often employed in thin slab casting.

Table 1. The common chemical composition of mold flux (Kromhout, 2011)

Main components		
component	**amount (wt%)**	**raw materials**
SiO_2	25-36	wollastonite, quartz
CaO	27-34	wollastonite, calcite
Al_2O_3	2-6	feldspar,cryolite
Na_2O	10-17	natrite, feldspar, cryolite
F	6-9	fluorite, cryolite
C_{free}	1-7	carbon black, graphite, coke
Minor components		
component	**amount (wt%)**	**raw materials**
MgO	<4	periclase, forsterite
TiO_2	<1	*
Fe_2O_3	<2	*
MnO	<4	pyrolusite
K_2O	<1	*
Li_2O	<1	spodumene

*: by raw materials or steel-slag interaction

As previously mentioned, the composition of mold flux includes various elements, each influencing crucial slag properties like viscosity, crystallization behavior, and the temperatures at which break and solidification occur (Kromhout, 2011). Table 2 illustrates the impact of various chemical compositions on the key physical features.

Table 2. Impact of various chemical constituents on the parameters of continuous casting mold fluxes (Mills & Fox, 2003).

Property /Constituent	CaO	SiO_2	Al_2O_3	MgO	Na_2O $+K_2O$	FeO	CaF_2	MnO	B_2O_3	ZrO_2
Viscosity	↓	↑	↑	↓	↓	↓	↓	↓	↓	↔
T_{br}	↑ (+8.7)	↓ (-3.3)	↓ (-8.4)	↓ (-13.8)	↓ (-3.2)	↓ (-18.4)	↓ (-6.5)[c]	↓ (-3.2)	↓	↑ (+10)
T_{sol}	↑	↓	↓ (-1.4)	↑ (-2.1)	↓ (-4.5)		↓ (-8.5)	↓	↓ (-15.3)	↑
Crystallisation Tendency	↑	↓	↓	↑	↑		↑	↑	↓	↑

where:

T_{br} (Break Temperature) = 1393K - %MO

T_{sol} (Solidification Temperature) = 1515K – x (MO)

(x: mole fraction, MO: oxide, ↑: increase, ↓: decrease and ([c]) refer to %F)

The point below which the viscosity of mold flux dramatically increases and the slag begins to behave non-Newtonianly is known as the break temperature. In industrial applications, this temperature is critical because it helps control mold lubrication and heat transmission. In the continuous casting process, longitudinal cracking and sticker breakouts can be avoided with careful management of the break temperature (Mills & Fox, 2003; Sridhar, Mills, Afrange, Lorz, & Carli, 2000). During measurements, it has been noted that variables like fluorine loss and cooling rate affect the break temperature. Furthermore, using certain equations, the break temperature values can be calculated within a ± 20K range based on the chemical composition of the mold flux (Mills, Yuan, Jones, 2011).

$$T_{br}(K) = 1393 - 8.4\%Al_2O_3 - 3.3\%SiO_2 + 8.65\%CaO - 13.86\%MgO - 18.4\%Fe_2O_3 - 3.2\%MnO - 9.2\%TiO_2 - 2.2\%K_2O - 3.2\%Na_2O - 6.47\%F$$

REFERENCES

Arefpour A., Monshi A., Khayamian T. and Saidi A.. (2012). Investigation of Viscosity's Effects on Continuous Casting of Steel Mold Fluxes Containing B2O3, Li2O, TiO2, Fe2O3, ZnO, and Na2O. Scientific Research, 4(08), 435-444.

Assia H. and Adel B.. (2012). Mold fluxes in continuous casting. IJRR, 2(1), 1-4.

Brandaleze E., Di Gresia G., Santini L., Martin A. and Benavidez E.. (2012). Mold Fluxes in the Steel Continuous Casting Process. In Science and Technology of Casting Processes (pp. 205-233). InTech.

Bothma J. A.. (2006). Heat transfer Through Mold Flux With Titanium Oxide Additions. South Africa: University of Pretoria.

Cruz A., Chavez F., Romero A., Palacios E. and Arredondo V.. (2007). Mineralogical phases formed by flux glases in continuous casting mold. Journal of Materials Processing Technology, 182(1-3), 358-362.

Elahipanah Z.. (2012). Thermo-Physical Properties of Mold Flux Slags for Continuous Casting of Steel. Royal Institute of Technology.

Kromhout J. A.. (2011). Mold fluxes for high speed continuous casting of steel. Gildeprint Drukkerijen.

Kromhout J. A.. (2013). Mold Flux Development for Continuous Casting of Steel. Transaction of the Indian Institute of Metals, 66(5-6), 587-596.

Mills K. C.. (2003). Mold Fluxes for Continuous Casting. Pittsbrugh: The AISE Steel Foundation.

Mills K. C. and Fox A. B.. (2003). The Role of Mold Fluxes in Continuous Casting- So Simple Yet So Complex. ISIJ International, 43(10), 1479-1486.

Mills K. C., Fox A. B., Thackray R. P. and Li Z.. (2004). The performance and properties of mold fluxes. VII International Conference on Molten Slags Fluxes and Salts (pp. 713-721). The South African Instute and Metallurgy.

Mills K.C., Yuan L., Jones R.T.. (2011). Estimating the physical properties of slag. The journal of Southern African Institute of Mining and Metallurgy, 111.

Mills K. C.. (2017). A short history of mold fluxes. Ironmaking & Steelmaking, 44(5), 326-332.

Samrudhi Engineers. (2022, July 25). The role of electromagnetic stirring in the continuous casting process. Samrudhi Engineers. https://samrudhiengineers.co.in/blog/the-role-of-electromagnetic-stirring-in-the-continuous-casting-process/

Saraswat R., Fox A. B., Mills K. C., Lee P. D. and Deo B.. (2004). The factors affecting flux consumption of mold fluxes. Scandinavian journal of metallurgy, 33(2), 85-91.

Sighinolfi D. and Paganelli M.. (2011). Study of the behaviour of mold fluxes for continuous casting by using the heating microscope. Innovation in Refractories and Traditional Ceramics.

Sridhar S., Mills K. C., Afrange O. D. C., Lorz H. P., and Carli R.. (2000). Break temperatures of mold fluxes and their relevance to continuous casting. Ironmaking and Steelmaking, 27(3), 238-242.

Wei E. F., Yang Y. D., Feng C. L. and Sommerville I. D., McLean A.. (2006). Effect of Carbon Properties on Melting Behavior of Mold Fluxes for Continuous Casting of Steel. Journal of Iron and Steel Research, 13(2), 22-26.

Wolf M. M.. (2003). Making, Shaping and Treating of Steel: Casting Volume. Pittsburgh: AISE.

Yan W., Yang Y.D., Chen W.Q., Barati M. and McLean A.. (2016). Design of mold fluxes for continuous casting of special steels. The Canadian Journal of Metallurgy and Materials Science, 54(4), 467-476.

FORMATION OF BORON NITRIDE IN THE PRESENCE OF TRANSITION METAL NITRATES IN MODERN MATERIALS SCIENCE

Muhammed ÖZ[1]

Ali Serol ERTÜRK[2]

Ümit ERDEM[3]

1. INTRODUCTION

The findings of contemporary materials science unequivocally illustrate the abundant conditions necessary for promising practical use (Ateş, 2016). Boron compounds exemplify this concept which are principally supplied from underground mineral resources and then, they are converted in high purity after enrichment processes. Boron is found in nature 230 different types of minerals most important commercial ones are tincal, colemanite, ulexite, probertite, boracite, hydroboracite and kernite. In addition to naturally occurring compounds of boron, there are also

1 Assoc. Prof. Dr. Bolu Abant İzzet Baysal University, Gerede Vocational School, Chemistry and Chemical Processing Technology, oz_m@ibu.edu.tr, ORCID: 0000-0003-0049-0161.

2 Assoc. Prof. Dr Ali Serol ERTÜRK, Adıyaman University, Department of Analytical Chemistry, Faculty of Pharmacy, aserturk@gmail.com, ORCID: 0000-0001-5352-7939.

3 Assoc. Prof. Dr. Kırıkkale University, Kırıkkale Vocational School, Department of Electronıcs and Automation, erdem.umit@gmail.com, ORCID: 0000-0002-0480-8176.

synthetically produced compounds. Boron nitride (BN), which contains crystal structures like carbon allotropes, is one of the most widely produced artificial boron compound. In addition, BN is famous compound that has gathered more attention on the science and technology for its significant role in engineering and widespread presence in daily life. BN stands for adaptability acting as a durable solid lubricant, a structural ceramic, a thermally conductive polymer additive, and a substrate for graphene-based films (Kimura et al., 1999; Sarıtekin, 2016; Naclerio, & Kidambi, 2023). However, the pursuit of simple, energy-efficient, and dynamically regulated methods to obtain powdery initial materials, which act as the foundation for easy synthesis of the mentioned BN material, is of principal importance in the field of materials science (Yoo, Akella, Cynn, & Nicol, 1997). Well-known representatives of this compound are cubic boron nitride and hexagonal boron nitride Paine, & Narula, 1990). Cubic boron nitride is a strong, hard, heat-resistant, refractory insulator. It is used as an abrasive and in tool manufacturing (Badzian, 1981; Sachdev, Haubner, Nöth, & Lux, 1997). Hexagonal boron nitride is an insulator with a large band gap, making it an important material for electronic device applications, similar to the development of graphene. This is often used in the form of a lubricant, in thermally conductive fillers, and also as a protective barrier layer. Films and plates of hexagonal boron nitride are transparent in the infrared and become transparent in the visible range after UV illumination.

The specific areas of practical use for hexagonal form of BN are supported by a combination of unique physical and chemical properties, including weak interatomic

interaction, minimal thermal expansion, negligible afterglow, and partial thermal conductivity (Haubner, Wilhelm, Weissenbacher, Lux, 2002; Bernard, Salameh, & Miele, 2016). It is important to emphasize that hexagonal BN (hBN) is the leading thermally conductive dielectric, as well as an essential amphoteric ceramic. hBN has shown a wide array of promising properties, some of which are similar to graphene while others are distinct and unattainable in graphene, at the perspective of materials research (Bartnitskaya, et al., 1996). Besides, hBN has proven to be a versatile material, especially in the area of monolayer hBN, also known as white graphene. This form of hBN has gathered attention due to its potential as a dielectric, its ability to form van der Waals heterostructures, its efficiency as a UV sensor, and other applications (Wu et al., 2017; Zhang, Penev, & Yakobson, 2017; Huang, & Li, 2018). In other words, hBN is a unique two-atom-thick insulator with a band energy just below that of a silicon derivative. Due to these properties, hBN plays key roles in the development of electronic devices in the nanometer scale range. However, to replace the silicon-based device structure, it is crucial to find a new structural material with similar electrical properties at its two-dimensional limit. Nevertheless, the experimental research in two-atom-thick hBN was much delayed, since the best material for hBN synthesis is, in fact, graphite, which requires carbon elimination for the reaction with boron. Hexagonal close-packed boron, a commonly available form of boron, has the ideal crystalline configuration, but the simplification of its crystalline structure limits the

opportunities for BN growth (Hagio, Nonaka, & Sato, 1997).

Another significant feature of hBN is to have a high thermal conductivity, which exceeds the thermal conductivity of the majority of metals at 300–400 K. This thermal conductivity is realized with a very low concentration of impurities in the hexagonal boron nitride, making it a very efficient and lightweight thermal insulator. Hexagonal boron nitride is stable in air up to 1000 °C, inert in different environments in a wide temperature range, and its structure and properties change only after heating to very high temperatures in a vacuum (Öz, M. 2020). It can be produced without any additional annealing. Due to this, hBN is used as a matrix for ceramic composites at high temperatures, where effective cooling and blending of materials are required (Malmqvist, & Tegman, 1997).

Initially, the availability of high-quality (especially high crystalline) hBN seemed unchallenging. However, limited access to high-quality material and subsequent difficulties in its commercial distribution became a notable hindrance as research on hBN-based devices progressed. Overcoming these obstacles is crucial to achieving significant accomplishments in hBN and its derivatives research. It has become evident that the advantageous properties of hBN require experimental validation from diverse research groups spanning various scientific disciplines such as solid-state chemistry, materials science, optoelectronics, photonics, power devices, and engineering. Collaboration is essential to prevent the isolation of individual hBN advancements and ensure

comprehensive exploration and understanding of this promising material. In principle, the availability of high-quality hBN in sufficient quantities is crucial for success in future research attempts (Yuan, et al., 2008). Studies' focus will be on identifying weaknesses in the hBN synthesis process, addressing these issues effectively, and anticipating a significant improvement in the accessibility of higher quality BN in presence of transition metal nitrates (TMN). This improvement will accelerate advancements in BN and various research fields derived from this material. Moving forward, a look into the fundamentals of BN will further shed light on this intriguing domain of scientific investigation.

The synthesis of BN can be approached through several methods. The most popular methods for the synthesis of h-BN are chemical vapor deposition, plasma-assisted methods, ion-beam synthesis, and solid state self-assembly. One of them involves the reaction of boron precursors with nitrogen sources in the presence of metal nitrates that is chiefly known as solventless solid state synthesis. Metal nitrates not only serve as nitrogen donors but can also influence the morphology and properties of the resultant boron nitride. Also, the incorporation of metal nitrates can lead to the formation of composite materials, enhancing the thermal and mechanical properties of boron nitride and expanding its application potential.

The investigation into the interaction between boron oxide and ammonia within a TMN powder resulted in the production of a finely dispersed combination of BN with metal oxides, amorphous boron oxide, and metal nitride. It

has been observed that the surface acidity of metal oxides, typically in the form of nitrates, nitrites, and halo complexes, significantly impacts the rate of the reaction and the quantity of gaseous products generated (Ateş, 2013). Furthermore, the use of metal oxides with the necessary d-electron level alters their influence on the organic reaction. In the context of synthesizing powdery hBN formulations, the modification of the reaction process will serve as a critical factor in comparing metal nitrates versus metal oxides. This study aims to explore the crystalline structure, the morphology and the formation of BN in the presence of various TMN, examining the resultant material properties by instrumental methods. One can optimize synthesis conditions to alter boron nitride's characteristics for specific industrial applications, covering the way for innovative advancements in material science.

2. MATERIALS AND METHODS

The samples were produced from commercial starting materials, namely boron oxide and urea, which are the primary precursors for boron nitride synthesis via solid-state production (O'Connor, 1962). The amounts of boron oxide, urea, and carbon were adjusted to 1.0 g, 2.0 g, and 0.03 g (w/w), respectively. The carbon content in the mixture was held constant at 0.03 g for all samples. Subsequently, additional additives, comprising metal nitrates ($Mx(NO_3)_x$, where M represents Ag, Fe, or Cu), were incorporated into the boron oxide-urea-carbon mixture at a concentration of 1% (w/w). The starting materials—boron oxide, urea, and carbon—were initially

mixed using a ball mill for 1 hour. This was followed by a high-temperature annealing process conducted at 1450 °C under an ammonia atmosphere (Öz, Saritekin, Bozkurt, & Yildirim, 2016). After cooling to room temperature, a bleaching step for the samples was performed using a 1 M hydrochloric acid solution. The primary characterization of the solid powder samples employed various instrumental methods. X-ray diffraction analysis (XRD) was primarily utilized for the qualitative detection of the formation of metal nitride-doped boron nitride in this study. XRD measurements were conducted using a Rigaku Multiflex diffractometer with a CuKα target, providing a monochromatic beam at 1.54 Å under standard conditions. The scan speed was set to 5°/min, covering the 2θ range from 10° to 90°. Fourier transform infrared spectroscopy (FTIR) was employed to detect the vibrational modes of the bonds present in the compounds, using a Shimadzu 8400S FTIR spectrophotometer. FTIR analysis was specifically applied to the carbon-doped samples to identify the bonding modes of boron nitride.

3. RESULTS AND DISCUSSION

In this study effect of both carbon and metal nitrates on the formation of the BN has been investigated details in the sight of the XRD examination. Carbon element was added to starting plain mixture for it has holistic mission in the medium. It was thought that the carbon element in the mixture would contribute positively to the formation of the BN due to its reducing feature. It was also expected that the reaction would occur faster by expanding the reaction

surface area because the BN possibly starts to occur BN macromolecules at the solid gas interface(Oz, 2020). Carbon in the medium decomposes to form carbon dioxide by removal of the oxide part of both boron oxide and metal nitrates as the main purpose of the synthesis BN includes principally decomposition of boron oxide and elimination of oxide compounds. In addition, not only the metal nitrates increase the reaction interface but also it was a possible source for nitrogen in the reaction blend. The chosen metal salts were Ag, Fe, or Cu nitrates that they have unique features in the environment. In the view of electronic structure whole are placed at the transition series of the periodic table. However, they are distinct from each other by the electron numbers at valence d-orbitals as 10, 9 and 5, silver copper and iron respectively.

XRD method has been known as the instrumental way of analysis by use of an X-ray source as copper that targets sample and then detects reflection. A formula was developed for each crystal unit to determine d spacing values for solid samples. The distance of Miller planes that present in the sample has unique and quantized values which were then used to determine the d-spacing of the atoms in the sample. Lattice parameters of solid samples, especially a, b, and c are also investigated via the XRD diffractograms.

FTIR spectra of the carbon containing samples principally includes the 795 (for BN), 1389 (for BN) and 3410 (for BOH or NH) cm^{-1} wavenumbers for lateral structure which were designated as out of plane, in plane and tip groups, respectively (Fig. 1). Shoulder peaks which

were mainly under the broad out of plane vibration modes, is observed at 1100 cm^{-1} is attributed as unreacted boron oxide starting material (Fig.1). The other metal added samples were expected to be similar peaks as well in plain mixture. This FTIR spectra is stemmed from a sign of transition from irregular to regular structure. In other words, it begins the transformation from turbostratic structure to hexagonal structure (Thomas, Weston, & O'connor, 1962). Although it shows the transition to a regular structure, the abundance of end groups still shows that the resulting product is mainly composed of a turbostratic nature (Jähnichen et al., 2022).

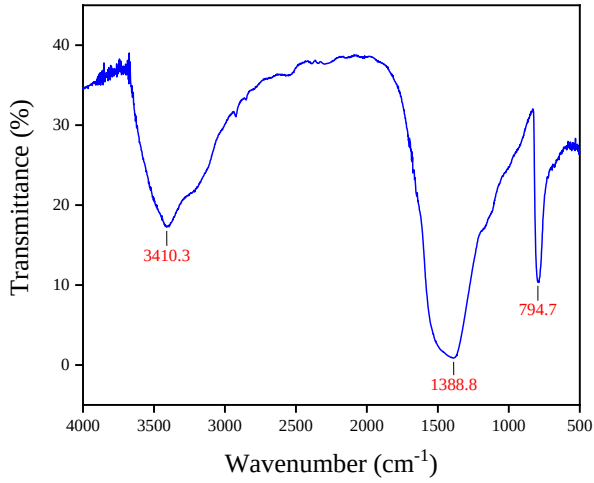

Fig. 1. FTIR spectra of plain mixture of the boron oxide urea and carbon triple system.

The main concept of this study is to determine the BN formation by XRD analysis (Balint, & Petrescu, 2009). Therefore, samples were analysed and their diffractograms are given in Fig. 2. The strong glimpse of the formation is to get an observable 002, 10X, 004 and 110 Miller indices. The 002 plane is the main plane while 10X plane

abbreviated for the combination of 100 and 101 planes. It is understood that the whole samples contain 002, 10X and 110 peaks however only plain mixture and iron nitrate added sample composed of all observable (Fig. 2) Miller indices. 004 peak in the iron nitride doped sample has the greatest intensity among the samples as well 002 peak. It is obvious that the electronic interaction of the d electrons at the valence shell of the metals is significantly important. Because the iron nitrate has half-filled valence d-orbital while silver nitrate full-filled d-orbitals. The number of lone electrons at the d-orbital positively affect the formation of BN.

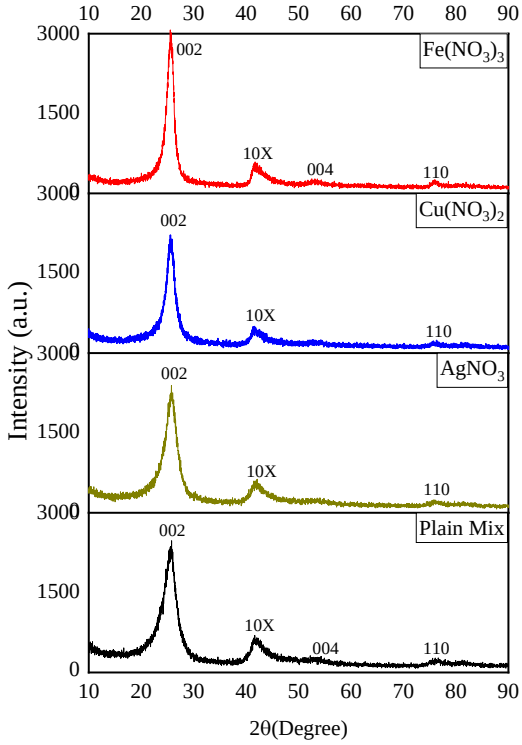

Fig. 2. Diffractograms of the metal nitrate doped BN at constant carbon concentration.

The numerical values of the XRD analysis are given in Table 1. This table was prepared from the diffractograms of each sample that it contains peaks' 2θ, d(Å), (hkl), height, Area, I % and FWHM values. These are utilized for the identification of the materials. The main peak (002) for BN is observed approximately at 25.7°, 100 % intensity for the samples under the consideration. In addition, the d parameter can be determined along with the a, b, and c parameters from the table. The a and b lattice units are equal and obtained from the peak observed about at 76.0° 2θ degree. It was found from the calculation of hexagonal system formulas as 2.48, 2.50, 2.51 and 2.51 Å for plain mixture, silver, copper, and iron nitrate respectively. The "c" lattice unit is also computed from this formula by help of the 002-plane observed at the 25.7° 2θ degree and it was found as 6.90, 6.92, 6.84 and 6.91 Å for plain mixture, silver, copper, and iron nitrate respectively. These results show that BN was successively synthesized however, there was a deviation from the hexagonal structure and the structure still remained in the turbostratic structure (Alkoy, Toy, Gönül, & Tekin, 1997). It has been observed that there is more transition to the ordered hexagonal structure thanks to the metal additive. Especially the amount of transformation of the structure into the structure has increased even more when iron nitrate is used.

To sum up, it can be said that the boron nitride formed according to the X-ray results is mostly turbostratic in structure when we analyse the data totally, but hexagonal structures are also observed. The added metal nitrates have a positive effect although it has very low amount in the reaction medium as 1%. It is predicted that

BN with a full hexagonal crystal structure can be obtained with the increase the amount of metal nitrates in the reaction blend (Yazdan, Hu, Nan, & Li, 2021). In addition, the electronic interaction of d orbitals of metals with the boron oxide, urea and carbon mixture mostly affects in a better way of formation BN.

Table 1. The diffractogram data of each sample obtained from Jade program (Jade Pro, 2019).

	2θ	d (Å)	(hkl)	Height	Area	I %	FWHM
Carbon	25.78	3.4529	002	191	10027	100	0.992
	41.621	2.1681	10X	45	2500	24.9	0.944
	54.339	1.6869	004	14	238	2.4	0.289
	76.675	1.2418	110	12	620	6.2	0.878
Silver (I) Nitrate	25.74	3.4582	002	211	11905	100	0.959
	41.498	2.1742	10X	35	1438	12.1	0.698
	76.038	1.2506	110	11	560	4.7	0.865
Copper (II) Nitrate	25.999	3.4243	002	258 28 15	20149	100	1.328
	41.778	2.1603	10X	28	1737	8.6	1.055
	75.702	1.2553	110	15	512	2.5	0.58
Iron (III) Nitrate	25.74	3.4582	002	407	22225	100	0.928
	41.539	2.1722	10X	77	4797	21.6	1.059
	52.94	1.7281	004	9	443	1.4	0.837
	75.819	1.2537	110	19	1131	5.1	1.012

4. CONCLUSION

XRD analysis of boron nitride was successfully performed to determine the effect of the carbon and metal nitrates on the boron nitride formation. The amount of the additives was adjusted very low approximately 1 % to save the purity of the formed sample from the contaminations.

According to the x-ray results, it was observed that the formed boron nitride was in a turbostratic structure, and the highest regular structure was obtained when iron (III) nitrate was added. In addition, all samples improved structure positively with respect to the plain mixture while iron (III) nitrate has the greatest contribution. The charges of the metals could be affectable on the improvement of the planar structure. Electronic interactions of the valence d orbitals of the metals give rise to an improvement on BN formation due to both the number of electrons exists in the d orbital and the nitrogen atoms which are present in metal nitrates.

REFERENCES

"JADE Pro ." 2019. Livermore, CA, USA.: MDI Materials Data.

Alkoy, S., Toy, C., Gönül, T., & Tekin, A. (1997). Crystallization behavior and characterization of turbostratic boron nitride. Journal of the European Ceramic Society, 17(12), 1415-1422.

Ateş, A. (2013). The Effect of Polymer-Cement Stabilization on the Unconfined Compressive Strength of Liquefiable Soils. *International Journal of Polymer Science*, *2013*(1), 356214.

Ateş, A. (2016). Mechanical properties of sandy soils reinforced with cement and randomly distributed glass fibers (GRC). *Composites Part B: Engineering*, *96*, 295-304.

Badzian, A. R. (1981). Cubic boron nitride-diamond mixed crystals. Materials Research Bulletin, 16(11), 1385-1393.

Balint, M. G., & Petrescu, M. I. (2009). An attempt to identify the presence of polytype stacking faults in hBN powders by means of X-ray diffraction. Diamond and related materials, 18(9), 1157-1162.

Bartnitskaya, T. S., Kurdyumov, A. V., Lyashenko, V. I., Ostrovskaya, N. F., Rogovaya, I. G. (1996). Catalytic synthesis of graphite-like boron nitride. Powder Metallurgy and Metal Ceramics, 35(5-6), 296-300.

Bernard, S., Salameh, C., & Miele, P. (2016). Boron nitride ceramics from molecular precursors: synthesis, properties and applications. Dalton Transactions, 45(3), 861-873.

Haubner, R., Wilhelm, M., Weissenbacher, R., Lux, B. (2002). Boron nitrides: properties, synthesis and applications (pp. 1-45). Springer Berlin Heidelberg.

Huang, J., & Li, Y. (2018). BN embedded polycyclic π-conjugated systems: Synthesis, optoelectronic properties, and photovoltaic applications. Frontiers in chemistry, 6, 341.

Jähnichen, T., Hojak, J., Bläker, C., Pasel, C., Mauer, V., Zittel, V., Deneche, R., Bathen, D., & Enke, D. (2022). Synthesis of Turbostratic Boron Nitride: Effect of Urea Decomposition. ACS omega, 7(37), 33375-33384.

Kimura, Y., Wakabayashi, T., Okada, K., Wada, T., & Nishikawa, H. (1999). Boron nitride as a lubricant additive. Wear, 232(2), 199-206.

Malmqvist, J., & Tegman, R. (1997). Boron nitride coated ceramic crucible with a hole in the bottom—a new device replacing expensive crucibles for the preparation of fusion bead samples for X-ray fluorescence analysis. *Analytical Communications*, *34*(11), 343-350.

Naclerio, A. E., & Kidambi, P. R. (2023). A review of scalable hexagonal boron nitride (h-BN) synthesis for present and future applications. *Advanced Materials*, *35*(6), 2207374.

O'connor, T. E. (1962). Synthesis of boron nitride. Journal of the American Chemical Society, 84(9), 1753-1754.

Öz, M. (2020). Temperature dependency on crystallinity and durability of mineral dolomite doped nanocrystalline hexagonal boron nitride. Journal of Inorganic and Organometallic Polymers and Materials, 30(3), 758-766.

Öz, M., Saritekin, N. K., Bozkurt, Ç., & Yildirim, G. (2016). Synthesis of highly ordered hBN in presence of group I/IIA carbonates by solid state reaction. *Crystal Research and Technology*, *51*(6), 380-392.

Paine, R. T., & Narula, C. K. (1990). Synthetic routes to boron nitride. Chemical reviews, 90(1), 73-91.

Sachdev, H., Haubner, R., Nöth, H., & Lux, B. (1997). Investigation of the c-BN/h-BN phase transformation at normal pressure. Diamond and related Materials, 6(2-4), 286-292.

Sarıtekin, N. K., Bilge, H., Kahraman, M. F., Zalaoğlu, Y., Pakdil, M., Doğruer, M., Yıldırım, G., & Oz, M. (2016). Improvement of mechanical characteristics and performances with Ni diffusion mechanism throughout Bi-2223 superconducting matrix. In *AIP Conference Proceedings* (Vol. 1722, No. 1). AIP Publishing.

Thomas, J. R., Weston, N. E., & O'connor, T. E. (1962). Turbostratic boron nitride, thermal transformation to ordered-layer-lattice boron nitride. Journal of the American Chemical Society, 84(24), 4619-4622.

Wu, P., Yang, S., Zhu, W., Li, H., Chao, Y., Zhu, H., Li, H., & Dai, S. (2017). Tailoring N-Terminated Defective Edges of Porous Boron Nitride for Enhanced Aerobic Catalysis. *Small*, *13*(44), 1701857.

Yazdan, A., Hu, B., Nan, C. W., & Li, L. (2021). Synthesis of polycrystalline boron nitride nanotubes with Lead (II) oxide and Iron (III) nitrate nonahydrate as promoters. *Physica E: Low-dimensional Systems and Nanostructures*, *133*, 114788.

Yoo, C. S., Akella, J., Cynn, H., & Nicol, M. (1997). Direct elementary reactions of boron and nitrogen at high pressures and temperatures. Physical Review B, 56(1), 140.

Yuan, S., Zhu, L., Fan, M., Wang, X., Wan, D., Peng, S., & Tang, H. (2008). Fluffy-like boron nitride spheres synthesized by epitaxial growth. Materials Chemistry and Physics, 112(3), 912-915.

PROMPT ENGINEERING: EFFECTIVE COMMUNICATION WITH ARTIFICIAL INTELLIGENCE

Mahmut DİRİK[1]

1. INTRODUCTION

The rapid progress in artificial intelligence (AI) has brought forth groundbreaking advancements, among which Large Language Models (LLMs) stand out as transformative tools. These models, built on intricate deep learning frameworks and trained with vast datasets, possess an exceptional ability to process and generate text that mimics human language. Their application spans diverse fields, including education, healthcare, creative industries, and business services, offering new opportunities to innovate and solve problems. However, effectively utilizing these models goes beyond their technical capacity; it requires a structured approach to design the inputs that guide their responses.

1 Assoc. Prof. Dr., Sirnak University, Department of Computer Engineering, ORCID: 0000-0000-0003-1718-5075.

At the heart of this approach lies Prompt Engineering, a specialized method focused on crafting purposeful and strategic input prompts. This practice plays a critical role in directing LLMs to deliver responses that are precise, relevant, and aligned with specific objectives. By understanding the mechanics of how prompts shape model behavior, users can unlock their full potential, ensuring outputs are both meaningful and actionable.

This chapter provides a detailed examination of Prompt Engineering, starting with its foundational principles and moving toward practical implementation techniques. It explores how the clarity, structure, and intent of a prompt directly influences the model's performance, enabling users to tailor outputs for a variety of tasks. These tasks range from generating creative content to solving domain-specific problems and retrieving structured information. The discussion is enriched with real-world scenarios that illustrate how thoughtful prompt design can enhance the effectiveness of AI in solving practical challenges.

Furthermore, the chapter underscores the importance of Prompt Engineering in fostering human-centered AI interactions. By refining how humans communicate with LLMs, this discipline bridges the gap between complex AI systems and everyday applications, making advanced technologies accessible and intuitive. It demonstrates how carefully constructed prompts not only improve the accuracy and relevance of AI-generated content but also contribute to seamless and productive workflows.

In summary, Prompt Engineering is a critical enabler for maximizing the capabilities of Large Language Models. It transforms these models into powerful collaborators, capable of assisting in a wide range of contexts. This chapter aims to serve as a comprehensive resource for researchers, practitioners, and developers, equipping them with the tools and techniques necessary to harness the transformative power of LLMs through the strategic design of input prompts.

2. WHAT IS PROMPT ENGINEERING?

Prompt engineering is the art and science of crafting effective input prompts to guide AI models toward desired outputs. It involves designing precise instructions, queries, or examples that align with the task at hand, enabling models to produce accurate, relevant, and meaningful responses. This process bridges the gap between human intent and machine comprehension, making it a foundational aspect of utilizing LLMs effectively (Brownlee, 2021, OpenAI, 2020).

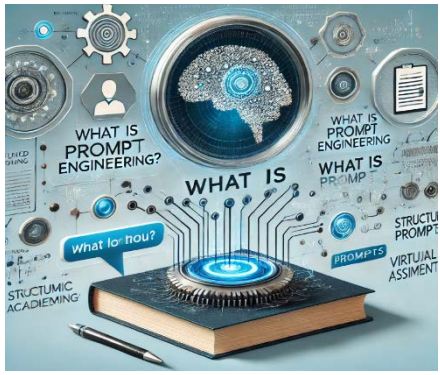

3. IMPORTANCE OF PROMPT ENGINEERING

The quality of an LLM's output is highly dependent on the structure and clarity of the input prompt. Poorly

constructed prompts can lead to irrelevant or erroneous outputs, while well-crafted prompts unlock the model's potential to generate insightful and creative content. Effective prompt engineering maximizes the utility of AI models, ensuring their outputs align with user objectives (Jurafsky & Martin, 2022).

4. HOW DO LARGE LANGUAGE MODELS WORK?

Large Language Models (LLMs) are advanced artificial intelligence systems trained on extensive text datasets using deep learning techniques. These models acquire the ability to identify linguistic patterns and relationships within the vast amounts of data they are trained on, enabling them to understand complex aspects of language such as grammatical structures, syntax, and semantic nuances. This ability allows LLMs to generate human-like text and accurately interpret the contextual meaning of language.

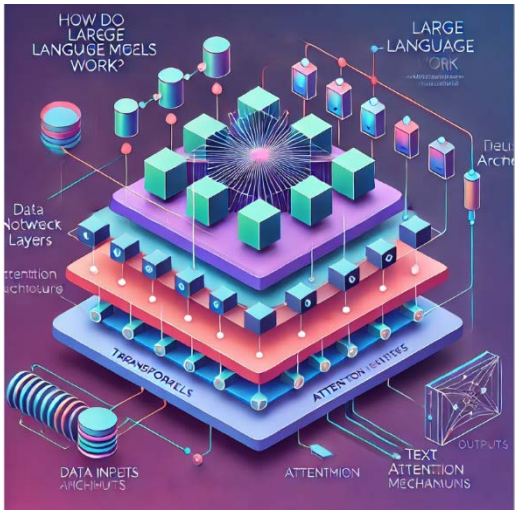

The foundation of LLMs' success lies in the transformer architecture, introduced by Vaswani et al. in their groundbreaking paper Attention Is All You Need. The

transformer represents a turning point in natural language processing, as it excels at effectively capturing long-range dependencies within text. While traditional methods often rely on sequential processing to understand linguistic context, the transformer architecture utilizes a self-attention mechanism that evaluates the contextual relationships among all words in a text simultaneously. This mechanism dynamically analyzes the importance of words or phrases relative to one another, ensuring that each contributes to the overall meaning.

The self-attention mechanism plays a crucial role in the ability of LLMs to comprehend linguistic context. By enabling each word or phrase in a text to be assessed in relation to the broader meaning, this mechanism ensures that the generated outputs are not only fluent but also contextually accurate. This structure allows LLMs to produce grammatically correct sentences while also interpreting complex expressions and providing responses suited to diverse contexts.

LLMs are effectively utilized in a wide range of applications, including text summarization, language translation, content generation, and dialogue systems. Thanks to the transformer architecture, these models can recognize not only short-range linguistic relationships but also long-term semantic connections within text, enabling them to produce richer and more contextually consistent outputs (Devlin et al., 2019), (Vaswani et al., 2017).

5. IMPACT OF PROMPTS ON MODEL PERFORMANCE

Prompts serve as pivotal mechanisms that direct the behavior and performance of AI models, exerting a profound impact on the quality and relevance of their outputs. Through the provision of well-defined instructions, contextual nuances, and specific constraints, prompts enable large language models (LLMs) to generate responses that are aligned with particular goals or requirements. The clarity and precision embedded in the prompt act as a framework that guides the model's decision-making process, ensuring that the generated content is not only coherent but also contextually appropriate and functionally effective. By carefully designing these prompts, practitioners can harness the full potential of LLMs, tailoring their outputs to address specific tasks, solve complex problems, or meet predefined criteria. This dynamic interaction between prompt formulation and model response underscores the critical role that prompt engineering plays in optimizing the efficacy of AI systems in real-world applications (Bengio et al., 2003).

6. CHARACTERISTICS OF EFFECTIVE PROMPTS

An effective prompt is essential for obtaining accurate and contextually appropriate outputs from LLMs. Key characteristics include:

- **Clarity:** Prompts must be explicit and unambiguous, leaving no room for misinterpretation by the model (Mikolov et al., 2013).
- **Specificity:** Providing sufficient context and constraints helps guide the model toward desired outputs (OpenAI, 2021).
- **Relevance:** The prompt should align with the model's training data and the task at hand to ensure meaningful results (Raffel et al., 2020).

Types of Prompts

Prompts can be categorized based on their structure and purpose:

- **Instructions:** Direct commands specifying the desired action for the model (Liang et al., 2021).
- **Questions:** Queries designed to extract specific information or insights (Salakhutdinov et al., 2020).
- **Examples:** Sample outputs provided to the model to illustrate the desired format or style (Strubell et al., 2019).
- **Scenarios:** Contextual setups that require the model to adopt a specific role or perspective (Wolf et al., 2020).

Techniques in Prompt Engineering

Prompt engineering employs both fundamental and advanced techniques to optimize model performance:

Basic Techniques

- **Zero-Shot Learning:** Instructing the model to perform a task without providing examples (Sutskever et al., 2014). **One-Shot and Few-Shot Learning:** Supplying one or a few examples to improve task understanding (Srivastava et al., 2015).
- **Chain of Thought Prompting:** Encouraging the model to break down complex tasks into smaller, manageable steps (He et al., 2016).

Advanced Techniques

- **Prompt Reformulation:** Iteratively refining prompts based on initial results to improve clarity and specificity (Zoph & Le, 2017).
- **Prompt Templates:** Creating reusable templates for recurring tasks (Radford et al., 2019).
- **Prompt Chaining:** Combining multiple prompts to achieve more complex objectives or multi-step outputs (Dosovitskiy et al., 2021).

Applications of Prompt Engineering

Prompt engineering plays a pivotal role in leveraging LLMs across diverse domains:

- **Text Generation:** Facilitating creative writing, translation, and summarization tasks (Howard & Ruder, 2018).
- **Question Answering:** Generating accurate responses to factual and open-ended queries (Graves et al., 2013).

- **Dialogue Systems:** Designing engaging and interactive chatbots and virtual assistants (Tay et al., 2020).
- **Code Generation:** Assisting in code completion and documentation (Bahdanau et al., 2015).
- **Data Analysis:** Enabling data exploration and interpretation (Koehn, 2009).

Ethical Considerations

As the field advances, prompt engineering must address key ethical challenges:

- **Bias and Fairness:** Ensuring prompts do not reinforce harmful stereotypes or biases inherent in training data (OpenAI, 2022).
- **Transparency:** Making AI outputs explainable and understandable for end-users (Koehn, 2009).
- **Misuse Prevention:** Avoiding prompts that generate misleading or harmful content (OpenAI, 2022).

7. CONCLUSION

Prompt engineering is not merely a technical skill; it is an interdisciplinary practice that blends linguistic precision with technological expertise. Mastering this field enables practitioners to effectively guide language models, unlocking their full potential and making them powerful tools for addressing real-world challenges. By understanding the intricacies of language and AI systems, skilled prompt engineers ensure that language models can

perform complex tasks with high accuracy, while also fostering the contextual awareness necessary for AI systems to respond appropriately to human-like reasoning and intent.

As AI becomes increasingly embedded in daily life, prompt engineering evolves beyond a mere technical necessity to become a core competency in optimizing human-AI collaboration, while maintaining ethical standards. This expertise plays a pivotal role in shaping how AI interacts with individuals, ensuring that systems respect societal, cultural, and ethical boundaries. Prompt engineering facilitates the navigation of nuanced communication, guiding AI to make informed decisions and provide relevant responses. The continued development of this skill set will be crucial in advancing AI systems that are not only effective in task execution but also capable of ethical and respectful interactions, marking a defining factor in the future trajectory of artificial intelligence.

REFERENCES

Bahdanau, D., Cho, K., & Bengio, Y. (2015). Neural machine translation by jointly learning to align and translate. In *Proceedings of the International Conference on Learning Representations (ICLR)*.

Bengio, Y., Ducharme, R., Vincent, P., & Janvin, C. (2003). A neural probabilistic language model. *Journal of Machine Learning Research, 3*, 1137–1155.

Brownlee, J. (2021). *Deep learning for natural language processing* (2nd ed.). Wiley.

Devlin, S., Chang, M.-W., Lee, K., & Toutanova, K. (2019). BERT: Pre-training of deep bidirectional transformers for language understanding. In *Proceedings of NAACL-HLT 2019*, Minneapolis, MN, USA.

Dosovitskiy, A., Beyer, L., Kolesnikov, A., Weissenborn, D., Zhai, X., Unterthiner, T., Dehghani, M., Minderer, M., Heigold, G., Gelly, S., Uszkoreit, J., & Houlsby, N. (2021). An image is worth 16x16 words: Transformers for image recognition at scale. In *International Conference on Learning Representations (ICLR)*.

Graves, A., Mohamed, A.-r., & Hinton, G. (2013). Generating sequences with recurrent neural networks. *arXiv.* https://arxiv.org/abs/1308.0850

He, K., Zhang, X., Ren, S., & Sun, J. (2016). Deep residual learning for image recognition. In *Proceedings of the IEEE Conference on Computer Vision and Pattern Recognition (CVPR)*.

Howard, J., & Ruder, S. (2018). Universal language model fine-tuning for text classification. In *Proceedings of the 56th Annual Meeting of the Association for Computational Linguistics (ACL)*, Melbourne, Australia.

Jurafsky, D., & Martin, J. H. (2022). *Speech and language processing* (3rd ed.). Pearson.

Koehn, P. (2009). *Statistical machine translation.* Cambridge University Press.

Liang, P., Chen, X., Yu, A. W., Yu, Z., Keutzer, K., & Darrell, T. (2021). LEGO: Learning fast modular task representations with prototypes. In *Advances in Neural Information Processing Systems (NeurIPS)*, vol. 34.

Mikolov, T., Chen, K., Corrado, G., & Dean, J. (2013). Efficient estimation of word representations in vector space. In *International Conference on Learning Representations (ICLR)*, Scottsdale, AZ, USA.

OpenAI. (2020). GPT-3: Language models are few-shot learners. *arXiv*. https://arxiv.org/abs/2005.14165

OpenAI. (2021). DALL·E: Creating images from text descriptions. *OpenAI.* https://openai.com/dall-e

OpenAI. (2022). Alignment research on AI systems: A comprehensive study. *OpenAI.* https://openai.com/research/alignment.

Radford, A., Wu, J., Child, R., Luan, D., Amodei, D., & Sutskever, I. (2019). Language models are

unsupervised multitask learners. *OpenAI.* https://openai.com/research/language-models

Raffel, C., Shazeer, N., Roberts, A., Lee, K., Narang, S., Matena, M., Zhou, Y., Li, W., & Liu, P. J. (2020). Exploring the limits of transfer learning with a unified text-to-text transformer. *Journal of Machine Learning Research, 21*, 1–67.

Salakhutdinov, R. R., Hinton, G. E., Krizhevsky, A., & Sutskever, I. (2020). Learning representations by back-propagating errors. *Nature Reviews Neuroscience, 21*(12), 667–676.

Srivastava, R. K., Greff, K., & Schmidhuber, J. (2015). Highway networks. In *Advances in Neural Information Processing Systems (NeurIPS)*, vol. 28.

Strubell, E., Ganesh, A., & McCallum, A. (2019). Energy and policy considerations for deep learning in NLP. In *Proceedings of the 57th Annual Meeting of the Association for Computational Linguistics (ACL)*, Florence, Italy.

Sutskever, I., Vinyals, O., & Le, Q. V. (2014). Sequence to sequence learning with neural networks. In *Advances in Neural Information Processing Systems (NeurIPS)*, vol. 27, Montreal, QC, Canada.

Tay, Y., Dehghani, M., Bahri, D., & Metzler, D. (2020). Long range arena: A benchmark for efficient transformers. *arXiv.* https://arxiv.org/abs/2011.04006

Vaswani, A., Shazeer, N., Parmar, N., Uszkoreit, J., Jones, L., Gomez, A. N., Kaiser, Ł., & Polosukhin, I. (2017). Attention is all you need. In *Advances in Neural*

Information Processing Systems (NIPS), Long Beach, CA, USA.

Wolf, T., Debut, L., Sanh, V., Chaumond, J., Delangue, C., Moi, A., Cistac, P., Rault, T., Louf, R., Funtowicz, M., & Rush, A. M. (2020). Transformers: State-of-the-art natural language processing. In *Proceedings of the 2020 Conference on Empirical Methods in Natural Language Processing (EMNLP)*, 38–45.

Zoph, H., & Le, Q. V. (2017). Neural architecture search with reinforcement learning. In *International Conference on Learning Representations (ICLR)*, Toulon, France.

COPPER-BASED COMPOSITE ELECTRICAL CONTACT MATERIALS PRODUCED BY POWDER METALLURGY METHOD

Yahya ALTUNPAK[1]

1. INTRODUCTION

Electrical contacts are key elements of elements such as contactors and relays. They are used in switching many power circuits such as electric motors, lighting, heating, capacitors, and switches. Electrical, thermal, chemical, and mechanical dynamic stresses occur in contact materials during opening-closing and short-circuiting. Since the contacts are constantly opening and closing, the electrical arcs that occur cause the contacts to oxidize and lose their conductivity over time. Consequently, a good contact material should have a high energy point, very good electrical and thermal conductivity, and be resistant to oxygen welding and high arc groups. [Wenge 2006]. With the development technology, contact needs have also changed. Especially in the aviation, automotive, and marine sectors, there is a need for materials that can combine features such as high performance, high strength, and stability at high temperatures.

[1] Prof Dr, Bolu Abant İzzet Baysal University, Department of Mechanical Engineering), altunpak_y@ibu.edu.tr, ORCID NO: 0000-0001-8676-4789.

In the selection of contact materials, the characteristics of the electrical circuit (current, voltage, etc.), the type of load, capacity, the force applied to the contacts, the number of opening and closing of the contacts, the frequency of opening and closing, and reliability are the main factors that should be taken into consideration [Young et al. 2012]. The current passing through the contacts is alternating or direct current, high or low value, and whether the load is inductive, capacitive, resistive, or a motor load is also important in material selection [Hidalgo-Manrique et al. 2019]. Many practical and experimental studies have been conducted to meet these needs. The main purpose of scientific studies in this field is generally to improve the performance (service life) of contact materials. Different chemical compositions, heat treatments, and mechanical or thermomechanical processes are tried to improve the mechanical, chemical, and physical properties of these materials.

Powder metallurgy techniques are generally used in the production of composite contact materials. To obtain the desired material properties with powder metallurgy production technique, the most appropriate process and output parameters must be researched and applied. In this study, firstly some developments in Cu-matrix composites are investigated. Then some powder production processes and other new production techniques which are preferred recently in literature are introduced. Then, some challenges related to high-performance Cu-matrix Electrical Contact Materials (ECMs) depending on the properties of different reinforcements are given.

2. ELECTRICAL CONTACT MATERIALS (ECMs)

ECMs are metal-based parts used to turn electrical circuits on and off at desired times (Figure 1). ECMs are widely used in electrical switches, electrical appliances, contactors, circuit breakers, voltage regulators, relays used to control electrical components in automobiles, relays for industrial purposes, and many other applications [Cantürk 2022], [Kesim 2018]. Electrical contacts can be examined in two groups moving and fixed contacts (Demir 1992). Fixed contacts are of suitable dimensions for short-circuit currents and are usually made of electrolytic copper. Moving contacts (sliding contacts) move during opening and closing. Therefore, the current transition point moves together with the moving contact. Moving contacts generally experience more wear and failure due to friction (Odabaşı 2017). Failure of electrical contacts can cause many accidents, including failure in city electricity lines, collapse of telephone infrastructure, and even loss of control of an aircraft flying in the air (Hiçyılmaz 1999).

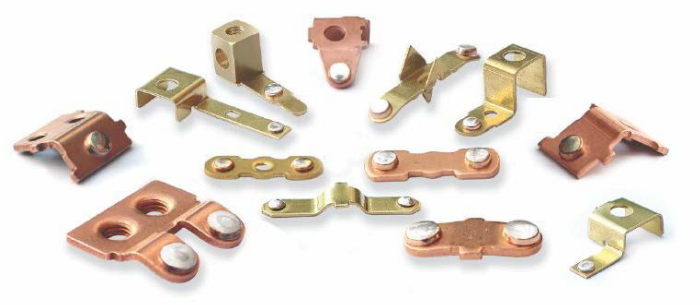

Figure 1 Some electrical contact materials used in industry

Electrical contact materials (ECMs), the heart of electrical contacts, determine the performance of devices. To meet the electrical contact requirements in applications, ECMs should have low contact resistance, superior thermal conductivity, and high mechanical (hardness and wear resistance) properties, as well as very good arc erosion resistance [Varol 2021, Güler 2021]. Therefore, copper matrix composites, which generally have both good electrical and thermal conductivity and good mechanical properties, have attracted the attention of many researchers [Zuo 2021, Jia 2022. Campbell, et al. 1998].

2.1. Copper Matrix Composite ECMs

Copper matrix composite ECMs are materials containing Cu matrix and reinforced with the second phase, such as metal oxides, ceramics, graphene, and carbon nanotubes on a metal matrix showing different chemical, physical, and mechanical properties. By adding some reinforcing elements to copper-based matrices, properties such as electrical, thermal, mechanical, and corrosion resistance of composite materials are improved. Different ECMs are preferred according to various current and voltage conditions. Especially in systems where high current is used, some hard metal and similar composites exhibit many features such as high electrical conductivity and thermal conductivity, high strength, and corrosion resistance should be used [Kesim et al. 2018]. There are numerous reports investigating the fabrication, modification, and degradation of copper matrix composite ECMs [Lungu 2019], [Hou et al. 2019]. Since copper-based

composite materials meet many of these conditions, they are used in many electrical applications (Allahverdiyev 2000, Hiçyılmaz 1999). Composites are the most ideal materials to meet such needs. Composite contacts are widely used in many devices such as heavy current-breaking contacts, circuit breakers, and fixed and moving contacts (Erbay 1998). In practice, Cu-based composite ECMs are mostly used in high-voltage electrical contact areas [Dong 2018, Liu 2021]. There are some studies on the fabrication techniques and corrosion behaviors of Cu-MC-ECMs [Lungu 2019, Lungu and Barbu 2022, Hou et al, 2019]. The powder metallurgy production method is mostly used in composite contact production (Deniz 2005). Such composite contacts can generally be used as a metal or metal alloy matrix, non-metallic compound, oxide, carbide, or nitride reinforcement phase. Thus, by producing a contact, a contact with high electrical and thermal conductivity and wear resistance, as well as resistance to arc erosion, is obtained (Edwards, Endean 1990). Arc erosion occurs as a result of material transfer from one contact to another due to the effect of adhesion and softening on the contact surfaces during the current flow while the contacts are opening and closing. Bu durum temasın ömrünü olumsuz yönde etkiler. (Allahverdiyev 2000). According to a study by Leung and his colleagues; the smaller the powder size, the slower the arc erosion rate. However, fine powders are not used much in the powder metallurgy method (smaller than 20 μm) since it is very difficult to prevent agglomeration in powders smaller than 20 μm during mixing (Bıyık & Aydın 2015).

These reinforcement elements or alloy atoms added to pure copper will disrupt the lattice structure and increase electrical resistance. Because electrical conductivity depends primarily on the mobility of electrons in the internal structure of a metal. In a microstructural study, it was stated that the regular structure of the SiC network surrounding the copper particles in samples with high SiC content sintered at relatively high temperatures was about to deteriorate. Irregular distribution of SiC reduced electrical conductivity more than regular distribution of SiC with the same content [Efe et al. 2010]. It has been stated that in SiC/Cu composites produced using the traditional powder metallurgy method, As the SiC content increased, density and electrical conductivity values decreased compared to unreinforced copper, but hardness and strength values increased [Efe et al. 2012]. When alumina is added to copper, the hardness increases and there is no significant decrease in electrical conductivity. In applications where electrical conductivity is important, the ceramic reinforcement ratio is around 1% (Aydın 1997).

Some of the advanced techniques used in powder metallurgy techniques have advantages and disadvantages below:

- The mechanical alloying technique has advantages such as interatomic diffusion; ultra-fine grain and nanoparticle production and disadvantages such as relatively low

preparation efficiency; and impurities easily entering the prepared powder.

- The spark plasma sintering (SPS) technique has the advantages of high preparation efficiency, relatively finer grains and higher interface bonding, but it is not good for industrial use.
- Internal oxidation technique has advantages such as coherent interface; improved interface wettability and fine oxide formation, but also disadvantages such as relatively complex higher cost due to the production process; and difficulty in controlling oxygen content.
- The in situ processing technique has advantages such as more consistent distribution, better control of process morphology, and simpler disintegration process, but disadvantages such as the absence of undesirable reactions and some incomplete reactions.

In order to prepare homogeneously dispersed high content nanocrystalline Y_2O_3/Cu composites, multi-step ball milling and reduction process was tried by subjecting CuO and Y_2O_3 mixtures to milling, reduction, secondary milling and annealing processes to homogeneously distribute high Y_2O_3 content in Cu matrix and refine the crystallite size of copper. A very good yield strength value (655 MPa) was obtained for the Y_2O_3/Cu composite material. Meanwhile, the electrical conductivity value decreased as expected by 53.8% IACS [Huang et al. 2019].

Although it can refine the composite grains by mechanical alloying using long-term ball milling technique, it significantly reduces the preparation efficiency. In addition, there is a risk of impurities entering the matrix, which may affect the properties of composites. In a study conducted on Nano ZrO_2 reinforced Cu-composites prepared by mechanical alloying; As the ZrO_2 content increased, the electrical conductivity and fracture stress values of the nanocomposite decreased, while the microhardness, compressive strength and yield strength values increased (Taha and Zawrah, 2017). In another study conducted by mechanical alloying, ın a study conducted by Moustafa and Taha on Cu matrix nanocomposites reinforced with nano-sized ceramic particles; grain refinement occurred as a result of severe plastic deformation occurring during mechanical alloying of composite powders. In addition, an increase in microstress and a decrease in grain size were observed in the Cu matrix in composites with high ceramic ratio [Moustafa and Taha 2021]. Very good strength and electrical conductivity values were obtained in Al_2O_3/Cu composites produced by internal oxidation and subsequent hot extrusion [Zhang et al. 2016]. In the internal oxidation method, which has the special ability to spontaneously produce oxide particles, oxygen is dissolved in the alloy powders and diffuses into the component phases, and more active elements react with oxygen to form uniformly distributed oxide particles. These oxidized alloy powders are then shaped by one of the appropriate conventional powder metallurgy methods (such as hot pressing and SPS [Zheng et al. 2019]. To

produce ultrafine-grained Al_2O_3/Cu bulk composites, Li et al. [Li et al. 2019] first dealloyed Al-Cu alloy powders to prepare nanocrystalline powders and then these powders were heat-treated. Then, they were consolidated by the powder compact extrusion method. It has been reported that Al_2O_3 nanoparticles in R1 heat-treated composites are generally distributed in grain boundaries, while Al_2O_3 nanoparticles in R2 heat-treated composites are generally distributed within grains and also have very good strength-ductility combination with high electrical conductivity values. In another study using the internal oxidation technique, CNTs with high surface cleanliness and high graphitization degree were evenly distributed on the surface of the composite powders and bonded well with the matrix. Then, CNTs/ Al_2O_3 /Cu bulk composites were sintered using the SPS technique [Guo et al., 2021]. In a study where Al_2O_3 dispersion reinforced Cu composites were obtained by using mechanical alloying, spark plasma sintering and hot extrusion methods, respectively, the microstructure of the composite materials produced by the combination of these methods consists of a heterogeneous microstructure consisting of coarse-grained Cu bands without Al_2O_3 and very fine-grained Cu regions rich in Al_2O_3. It has been stated that the existence of these different microstructural regions can be adjusted to obtain the desired mechanical and electrical properties [Zhou et al. 2018]. The presence of Al_2O_3 -free coarse-grained Cu bands in Al_2O_3 dispersion-strengthened Cu composite materials on the heterogeneous microstructure when strengthened by mechanical alloying, spark plasma sintering, and hot extrusion, the electrical conductivity

and tensile strength properties of the composite were improved. [Zheng et al. 2019]. In the bulk composites, CNTs well bonded with the Cu matrix and Al_2O_3 particles significantly improved the mechanical and electrical properties of the composite. Since Al_2O_3 and CNTs are distributed at the grain boundaries, grain growth in the Cu matrix is inhibited. In recent years, the in situ synthesis method developed for the production of Cu matrix composites is a new preparation technique used to form the desired reinforcement phases in the matrix by performing a series of thermo-mechanical processes or chemical reactions under certain conditions and thus to improve some desired properties of the composites [Zhang et al. 2022]. It has been stated that electrical and mechanical properties are improved in Cu alloys strengthened with TiC dispersion using a two-stage ball milling process followed by SPS techniques [Wang et al. 2014]. Very high mechanical and electrical conductivity values were obtained in 0.12% Al added CNT reinforced Cu-Al_2O_3 composites, which were successfully prepared by internal oxidation, chemical vapor deposition (CVD), and SPS methods [Guo et al. 2021]. Some ceramic reinforced Cu matrix composites prepared by various techniques are summarized in Table 1 [Yan et al. 2023]. It can be seen that Cu matrix composites prepared by different advanced techniques tend to exhibit particularly adequate strength and electrical conductivity. For example, 1.1Al_2O_3/Cu composite produced by internal oxidation followed by hot extrusion is observed to have improved strength and electrical conductivity properties [Zhang et al 2016].

2.2.Summary and future perspective

Although significant progress has been made in Electrical contact materials (ECMs) research in recent years, there are still some important challenges that need to be addressed. For example, in the mechanical alloying technique; impurities mixed into the powder, the spark plasma sintering technique is not good for industrial use, the internal oxidation technique has relatively complicated process and high cost; and in the in situ processing technique, the formation of certain reactants and incomplete reaction. In this research, various preparation processes and different preparation methods that can be used in the production of composites that can be used as electrical contact material (ECM) with Cu matrix ceramic particles distributed uniformly in the matrix were investigated. The effects of these new techniques and processes on the tensile, compressive and fracture strengths and electrical conductivity values of the produced composites were discussed. In general, research on ceramic-reinforced Cu matrix composites is ongoing.

Tablo 1: Summary of comprehensive properties of ceramics reinforced Cu matrix composites prepared by various processes. σ0.2: yield strength; CS: Compressive strength; TS: tensile strength.

Composites (wt%)	Production Techniques	$\sigma_{0.2}$ (MPa)	Electrical cond. (% IACS)	Ref.
3ZrO_2-Cu	Mechanical Alloying	61 (CS)	73,45	[Taha and Zawrah 2017]
5.9Y_2O_3-Cu	Mechanical Alloying + SPS	655 (CS)	53,8	[Huang 2019]
1SiC-Cu	Mechanical Alloying	48 (CS)	47,4	[Moustafa and Taha 2021]
3TiC-Cu	Mechanical Alloying + SPS	572 (TS)	71,5	[Wang et al. 2014]
Al_2O_3-Cu	Mechanical Alloying	600	89	[Çelebi Efe 2010]
2Al_2O_3-Cu	SPS (10 min) + hot extrusion	428 (TS)	87,1	[Zhou et al. 2018]
1Ti_2AlC/Cu	In-situ	118 (TS)	84,3	[Yan et al. 2021]+
1.1Al2O3-Cu	Internal oxidation + hot extruded	533 (TS)	85	[Zhang et al 2016]+
1.8La2O3-Cu	Internal oxidation + SPS	239 (TS)	93,1	[Zheng et al. 2019]+
34Al2O3-Cu	Internal oxidation + hot pressing	281 (CS)	86	[Zheng et al. 2019]+
1.6 Al2O3-Cu (R1)	Internal oxidation + heat treatment	335 (TS)	95	[Li et al. 2019]]+
0.12 Al2O3-Cu	Internal oxidation	163 (TS)	89	[Guo et al. 2021]+
1TiC-Cu	In-situ	281 (CS)	77	[Zhang et al. 2022]+

In particular, new manufacturing processes and reducing the disadvantages of these techniques while preserving their advantages will be the focus of further studies. Additionally, Cu matrix composites reinforced with materials with better conductivity such as high-performance CNTs, carbon fibers, and graphene will be among the priorities of future research.

REFERENCES

Allahverdiyev, Z.,(2000). Elektroteknik Malzemeleri, K.T.Ü., Trabzon.

Aydın, Ş.,1997, "Toz Metalurjisi Yöntemleri İle Elde Edilen Seramik Tanecik Destekli Alüminyum Esaslı Kompozit Malzemelerin Mekanik Özellikleri", Yüksek Lisans Tezi, Gazi Üniversitesi, Ankara.

Cantürk, S. B., & Kováčik, J. (2022). Review of recent development in copper/carbon composites prepared by infiltration technique. Energies, 15(14), 5227.

Çelebi Efe GF. Development of conductive copper composites reinforced with SiC. PhD Thesis. Sakarya University, Institute of Science and Technology; 2010

Demir, A., 1992, "Toz Metal Bir Çeliğin Mekanik Özellikleri", Yüksek Lisans Tezi, Gazi Üniversitesi, F.B.E, Ankara.

Deniz, M. E., 2005, Kompozit Malzemelerin Üretim Yöntemler Ve Isıl İşlemle Presleme Tekniğini Kullanarak Kompozit Malzeme Üretecek Bir Düzeneğin Tasarım Ve İmalatı, Yüksek Lisans Tezi, Harran Üniversitesi Fen Bilimleri Enstitüsü, Makine Mühendisliği Anabilim Dalı, Şanlıurfa.

Dong, L. L., Ahangarkani, M., Chen, W. G., & Zhang, Y. S. (2018). Recent progress in development of tungsten-copper composites: Fabrication, modification and applications. International Journal of Refractory Metals and Hard Materials, 75, 30-42.

Efe, G C., Altınsoy, G F., Yener, İ., T., İpek, M., Zeytin, S., & Bindal, C. (2010). Characterization of cemented Cu matrix composites reinforced with SiC.

Efe, G. C., İpek, M., Zeytin, S., & Bindal, C. (2012). An investigation of the effect of SiC particle size on Cu–SiC composites. Composites Part B: Engineering, 43(4), 1813-1822.

Erbay A.,1998,Endüstride Toz Metalurjisi ve Çeşitli Uygulamaları,Yüksek Lisans Tezi, Sakarya Üniversitesi.

Guo X, Chen X H, Liu P, Zhou H L, Fu S L, Li W, Liu X K, Ma F C and Wu Z P 2021 Preparation and mechanical properties of copper matrix composites reinforced by carbon nanotubes and Al2O3 Adv. Eng. Mater. 23 2001490

Güler, O., Varol, T., Alver, Ü., & Biyik, S. (2021). The wear and arc erosion behavior of novel copper based functionally graded electrical contact materials fabricated by hot pressing assisted electroless plating. Advanced Powder Technology, 32(8), 2873-2890.

Hiçyılmaz, N.,1999, "Toz Metalurjisi Yöntemi ile Elde Edilen Seramik Tanecik Destekli Alüminyum Esaslı Kompozit Malzemelerin Aşınma Özellikleri", Yüksek Lisans Tezi, Gazi Üniversitesi, Ankara

Hidalgo-Manrique, P., Lei, X., Xu, R., Zhou, M., Kinloch, I. A., & Young, R. J. (2019). Copper/graphene composites: a review. Journal of materials science, 54, 12236-12289.

Hou, C., Song, X., Tang, F., Li, Y., Cao, L., Wang, J., & Nie, Z. (2019). W–Cu composites with submicron-and nanostructures: progress and challenges. NPG Asia Materials, 11(1), 74.

Huang F, Wang H, Yang B, Liao T and Wang Z Y (2019) Uniformly dispersed Y2O3 nanoparticles in nanocrystalline copper matrix via multi-step ball milling and reduction process Mater. Lett. 242 119–22

Jia, C., Li, S., Guo, X., Wang, X., Su, J., & Song, K. (2022). Arc erosion resistance mechanism of Cf–Al2O3/Cu composites modified by carbon fibers. Journal of Materials Research and Technology, 19, 4957-4968.

Kesim, M. T., Yu, H., Sun, Y., Aindow, M., & Alpay, S. P. (2018). Corrosion, oxidation, erosion and performance of Ag/W-based circuit breaker contacts: A review. Corrosion Science, 135, 12-34.

Li C G, Xie Y H, Zhou D S, Zeng W, Wang J, Liang J M and Zhang D L 2019 A novel way for fabricating ultrafine grained Cu-4.5 vol% Al2O3 composite with high strength and electrical conductivity Mater. Charact. 155 109775

Liu, D. G., Zhang, P., Ruan, C. F., Meng, L., Luo, L. M., Wang, Z. M., & Wu, Y. C. (2021). Fabrication and characterization of W/Cu/Ni-based high specific gravity alloy with Zr and Ti combined addition. International Journal of Refractory Metals and Hard Materials, 101, 105674.

Lungu, M. V. (2019). Synthesis and Processing Techniques

of Tungsten Copper Composite Powders for Electrical Contact Materials A Review. Oriental Journal of Chemistry, 35(2).

Lungu, M. V., & Barbu, A. (2022). Graphene and its derivative reinforced tungsten–copper composites for electrical contact applications: A review. Journal of Reinforced Plastics and Composites, 41(15-16), 624-636.

Moustafa E B and Taha M A (2021) Evaluation of the microstructure, thermal and mechanical properties of Cu/SiC nanocomposites fabricated by mechanical alloying Int. J. Miner. Metall. Mater. 28 475–86.

Odabaşı, Ç., (2017), "Toz Metalurjisi ile Üretilen Nb-V Mikroalaşım Çeliğine Bakır İlavesinin Mikroyapı Mekanik Özellikleri Üzerine Etkisinin Araştırılması", Yüksek Lisans Tezi, Karabük Üniversitesi Fen Bilimleri Enstitüsü, Karabük.

Taha M A and Zawrah M F (2017) Effect of nano ZrO2 on strengthening and electrical properties of Cu-matrix nanocomposits prepared by mechanical alloying Ceram. Int. 43 12698–704

Varol, T., Güler, O., Akçay, S. B., & Aksa, H. C. (2021). The effect of silver coated copper particle content on the properties of novel Cu-Ag alloys prepared by hot pressing method. Powder Technology, 384, 236-246.

Wang F L, Li Y P, Yamanaka K, Wakon K, Harata K and Chiba A (2014) Influence of two-step ball-milling condition on electrical and mechanical properties of

TiCdispersion-strengthened Cu alloys Mater. Des. 64 441–9

Wenge, C. H. E. N., Zhanying, K., Hongfang, S. H. E. N., & Bingjun, D. I. N. G. (2006). Arc erosion behavior of a nanocomposite W-Cu electrical contact material. Rare Metals, 25(1), 37-42

Yan Y X, Zou J M, Zhang X H, Xiao Q, Chen B Q, Huang F, Li X X, Yang B and Liang T X (2021) Investigation on microstructure and properties of TiC0.5-Al2O3/Cu composites fabricated by a novel in-situ reactive synthesis Ceram. Int. 47 18858–65

Yan, Y. F., Kou, S. Q., Yang, H. Y., Shu, S. L., Qiu, F., Jiang, Q. C., & Zhang, L. C. (2023). Ceramic particles reinforced copper matrix composites manufactured by advanced powder metallurgy: Preparation, performance, and mechanisms. International Journal of Extreme Manufacturing, 5(3), 032006.

Young, R. J., Kinloch, I. A., Gong, L., & Novoselov, K. S. (2012). The mechanics of graphene nanocomposites: a review. Composites Science and Technology, 72(12), 1459-1476.

Zhang D D, He X Y, Zhao H and Gao Y L (2022) Properties of TiCp/Cu composites fabricated by powder metallurgy and electrodeless copper plating Mater. Sci. Technol. 38 5–11

Zhang X H, Li X X, Chen H, Li T B, Su W and Guo S D (2016) Investigation on microstructure and properties of Cu-Al2O3 composites fabricated by a novel in-situ reactive synthesis Mater. Des. 92 58–63

Zheng R G and Li N N (2019) Mechanical properties and electrical conductivity of nano-La2O3 reinforced copper matrix composites fabricated by spark plasma sintering Mater. Res. Express 6 106527

Zhou D S, Wang X K, Muránsky O, Wang X R, Xie Y H, Yang C and Zhang D L (2018) Heterogeneous microstructure of an Al2O3 dispersion strengthened Cu by spark plasma sintering and extrusion and its effect on tensile properties and electrical conductivity Mater. Sci. Eng. A 730 328–35

Zuo, H., Wei, W., Yang, Z., Li, X., Ren, J., Xian, Y., ... & Wu, G. (2021). Performance enhancement of carbon/copper composites based on boron doping. Journal of Alloys and Compounds, 876, 160213.

CALCULATING THE BIOMASS ENERGY PRODUCTION POTENTIAL FROM ANIMAL AND AGRICULTURAL WASTES IN ANKARA PROVINCE

Hamza ALAHMAD[1]

Edip TAŞKESEN[2]

1. INTRODUCTION

With the rapid growth of the global population, the demand for energy is also increasing. The main reasons for this rise in energy demand are industrialization and the desire to improve the quality of life (Holdren, 1991; Yağlı & Koç, 2019; Taşkesen et al., 2022). This demand affects the use of various energy sources such as fossil fuels, renewable energy sources (solar, wind, geothermal, etc.), and nuclear energy sources (Karaca, 2015). In 2023, 60.65% of global electricity was generated from fossil fuels, 30.24% from renewable energy, and 9.11% from nuclear energy. In Turkey, 57.99% of electricity came from fossil fuels, and 42.01% was derived from renewable sources. Fossil fuels are limited resources, and their continued use carries the risk of depletion.

[1] MSc. Eng., Şırnak University, Graduate School of Education, Energy Science and Technologies Program (MSc), hmza8246@gmail.com, ORCID: 0000-0002-6261-3449.

[2] Dr. Lecturer, Şırnak University, Faculty of Engineering, Energy Systems Engineering, edip.taskesen@sirnak.edu.tr, ORCID: 0000-0002-3052-9883.

The use of fossil fuels leads to the uncontrolled release of greenhouse gases, contributing to environmental pollution. The Kyoto Protocol and the Paris Agreement support global efforts to reduce greenhouse gas emissions. The European Green Deal aims for carbon-neutrality by 2050 and facilitates the transition to clean energy. Renewable energy sources play a key role in achieving these goals. Biomass energy has gained attention for its sustainable energy production and lower greenhouse gas emissions compared to other renewable energy sources. Biogas has become increasingly important, with countries like India and China prioritizing its production (Dhar, Kumar, & Kumar, 2017).

Recycling animal and agricultural wastes is important to prevent environmental issues such as health problems and odors. Instead of disposal, these wastes can be used in anaerobic processes for energy production, helping combat climate change. The purification of biogas obtained from waste fermentation can increase methane content and potentially reduce fossil fuel use and greenhouse gas emissions by 60-80% (Biogas for Road Vehicles: Technology Brief, 2017). Anaerobic digestion occurs in three stages (hydrolysis, acidogenesis, and methanogenesis) to produce biogas from organic waste (Vijin Prabhu, Sivaram, Prabhu, & Sundaramahalingam, 2021). Biogas contains methane, carbon dioxide, and trace amounts of other gases (Bharathiraja et al., 2018; Li et al., 2019; Robles, Nair, Kleinsteuber, Nikolausz, & Sárvári Horváth, 2018).

This study aims to investigate the biogas potential from animal and agricultural wastes in Ankara province. The theoretical biogas and energy potentials derived from these wastes have been calculated.

2. MATERIALS AND METHODS

2.1. Working Area

Ankara is located in the northwestern part of the Central Anatolia Region, between 39° 55' north latitude and 32° 50' east longitude. The province covers an area of 26,897 km² and has an average elevation of 890 meters above sea level. It is bordered by Kırşehir and Kırıkkale to the east, Eskişehir to the west, Çankırı to the north, Bolu to the northwest, and Konya and Aksaray to the South (Ankara Coğrafyası 2024, Genel Coğrafya ve Yeryüzü Şekilleri 2024). The population of Ankara is 5,803,482 (Adrese Dayalı Nüfus Kayıt Sistemi Sonuçları 2024). Figure 1 shows the map of Ankara and its districts.

Figure 1. Ankara province map.

2.2. Animal Population Data

In this study, data from 2023 provided by the Turkish Statistical Institute (TURKSTAT - TÜİK) central distribution system were used (Hayvancılık İstatistikleri, 2024). The amount of manure from cattle, ovine animals, and poultry in Ankara was calculated in the first phase of the study, and the resulting biogas potential was determined. The theoretical biomass potential of selected agricultural products, their annual production amounts, and the recoverable energy potentials of each waste were also calculated based on assumptions. According to the 2023 data, the total animal population in Ankara is 16,997,897, including 610,514 cattle, 1,879,395 ovine animals, and 14,507,988 poultry. The highest cattle farming occurs in the Central and Polatlı districts, while the Central district also leads in ovine animal farming, and Polatlı has the highest poultry farming (Fig. 2 and Table 1). The distribution of cattle, ovine animals, and poultry in Ankara is 85.4% poultry, 11% ovine animals, and 3.6% cattle.

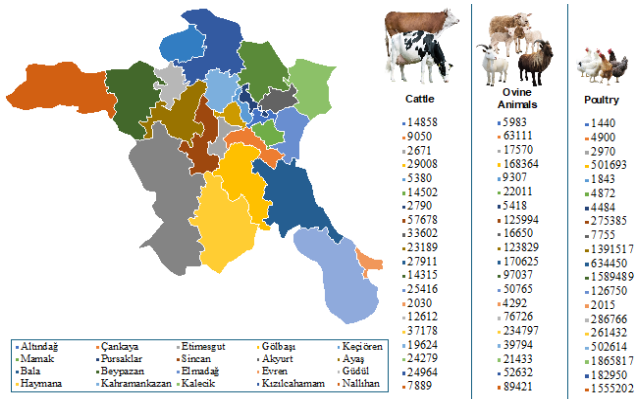

Figure 2. Potential map of cattle, sheep and poultry by districts in Ankara province (Number).

Table 1. Total number of animals in Ankara province (Hayvancılık İstatistikleri, *2024*).

District	Cattle	Ovine Animlas	Poultry
Center	135,937	417,758	797,587
Akyurt	33,602	16,650	7,755
Ayaş	23,189	123,829	1,391,517
Bala	27,911	170,625	634,450
Beypazarı	14,315	97,037	1,589,489
Elmadağ	25,416	50,765	126,750
Evren	2,030	4,292	2,015
Güdül	12,612	76,726	286,766
Haymana	37,178	234,797	261,432
Kahramankazan	19,624	39,794	502,614
Kalecik	24,279	21,433	1,865,817
Kızılcahamam	24,964	52,632	182,950
Nallıhan	7,889	89,421	1,555,202
Polatlı	122,879	344,277	3,711,922
Yenimahalle	2,931	9,184	2,340
Çamlıdere	14,324	12,096	4,225
Çubuk	70,925	38,981	1,577,515
Şereflikoçhisar	10,509	79,098	7,642
Total	**610,514**	**1,879,395**	**14,507,988**
Grand Total (Ankara Province)	**16,997,897**		

2.3. Agricultural Land and Crop Production Data

Ankara province covers a total area of 2,543,700 hectares (25,437,000 decares). According to the 2023 TURKSTAT-TUİK data, approximately 11,621,187 decares of this area is agricultural land, making up 45.7% of the total area of Ankara (Bitkisel Üretim İstatistikleri 2024). The distribution of agricultural lands by district is shown in Figure 3, and Table 2 provides the agricultural land sizes in decares by district. In 2023, 73% of the cultivated areas in Ankara are dedicated to grains and other crops, 21.7% are left fallow, 3.3% are planted with vegetables, 1.9% with fruits, beverages, and spices, and 0.003% with ornamental plants (Bitkisel Üretim İstatistikleri 2024). Figure 4 illustrates the distribution of cultivable areas by product group in Ankara province. The total production in Ankara city center and its districts amounted to 3,739,821 tons, with

approximately 94% of these products belonging to the grain group, the largest of which is wheat at 29.5%. Sugar beet follows at 23.5%, barley at 21%, and maize at 14%. Vegetables and fruits make up about 6% of the total production, with tomatoes at 3.4% and apples at 1.1%. The production quantities of grains, fruits, and other crops in Ankara province and its districts are detailed in Tables 3, 4, and 5.

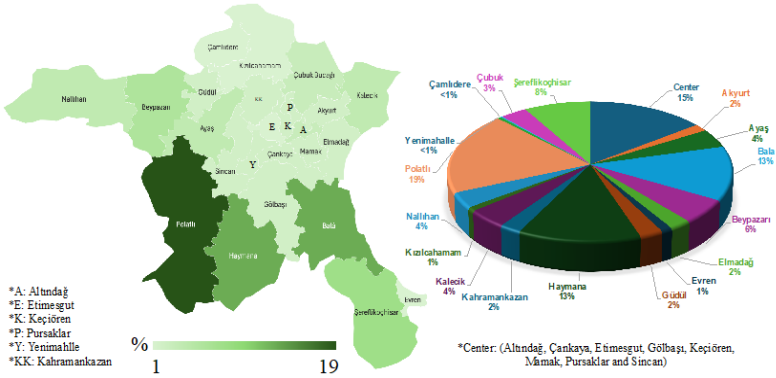

Figure 3. Proportional distribution of arable agricultural area by districts in Ankara Province in 2023 (Bitkisel Üretim İstatistikleri 2024).

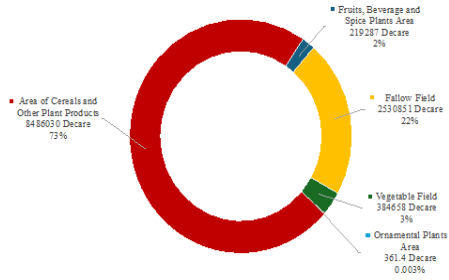

Figure 4. Cultivable agricultural area and rate in Ankara Province according to product group in 2023 (Bitkisel Üretim İstatistikleri 2024).

Table 2. Arable agricultural area in Ankara Province in 2023 (Bitkisel Üretim İstatistikleri 2024).

District	Area (Decare)
Center	1,700,423
Akyurt	197,009
Ayaş	510,544
Bala	1,461,051
Beypazarı	640,602
Elmadağ	269,486
Evren	137,518
Güdül	285,637
Haymana	1,489,152
Kahramankazan	263,658.5
Kalecik	495,299
Kızılcahamam	103,701
Nallıhan	413,255
Polatlı	2,219,467
Yenimahalle	54,015.9
Çamlıdere	24,526
Çubuk	391,129
Şereflikoçhisar	964,714
Total	**11,621,187.4**

Table 3. Production quantities of selected grain products according to Ankara Districts – tons (Bitkisel Ürün Denge Tabloları 2024).

District	Wheat	Barley	Sweetcorn	Bean	Rye
Center	176,223	132,181	63,145	7	110
Akyurt	18,295	11,656	4,315	5	-
Ayaş	57,157	54,369	132,876	92	-
Bala	75,506	85,011	37,675	6	75
Beypazarı	62,843	41,735	3,120	7	-
Elmadağ	18,552	15,108	1,350	19	25
Evren	13,198	10,848	423	193	-
Güdül	22,658	23,437	43,000	-	-
Haymana	156,525	113,122	27,100	210	38
Kahramankazan	22,713	15,484	25,780	54	-
Kalecik	44,305	23,138	26,035	3	255
Kızılcahamam	15,573	4,192	-	19	-
Nallıhan	30,214	22,587	15,313	88	131
Polatlı	318,762	107,573	116,474	64	75
Yenimahalle	5,151	1,940	-	-	-
Çamlıdere	639	425	-	8	18
Çubuk	23,447	19,037	8,250	105	9
Şereflikoçhisar	39,995	97,808	23,303	27	16
Total	**1,101,756**	**779,651**	**528,159**	**907**	**752**
Grand Total			**2,411,225 Tons**		

Table 4. Production quantities of selected grain products according to Ankara Districts – tons (Bitkisel Ürün Denge Tabloları 2024).

District	Sugar beet	Sorghum	Chickpeas	Oat	Potatoes
Center	96,078	320	17,234	11,070	1,210
Akyurt	-	-	4,345	67	8
Ayaş	24,501	88	11,421	1,067	570
Bala	56,019	-	1,980	10,497	11,209
Beypazarı	10,894	-	12,188	2,365	72
Elmadağ	1,025	-	1,414	1,470	-
Evren	2,778	-	1,579	-	-
Güdül	923	-	2,829	-	-
Haymana	61,367	-	14,025	25,150	76
Kahramankazan	16,683	-	2,035	3,333	1,051
Kalecik	70,514	-	2,746	753	894
Kızılcahamam	1,517	-	85	228	730
Nallıhan	1,671	-	308	783	1,401
Polatlı	374,533	-	2,622	5,264	16,058
Yenimahalle	-	-	324	-	-
Çamlıdere	-	-	7	1,260	30
Çubuk	-	-	3,135	777	701
Şereflikoçhisar	163,412	-	21,720	2,204	21,411
Total	**881,915**	**412**	**99,997**	**66,288**	**55,421**
Grand Total			**1,104,033 Tons**		

Table 5. Production quantities of selected vegetable and fruit products by Ankara Districts – tons (Bitkisel Ürün Denge Tabloları 2024).

District	Tomatoes	Cabbage	Apple	Grape	Cherry
Center	14,329	622	5,342	681	1,774
Akyurt	1,899	-	1,267	171	536
Ayaş	27,975	387	3,461	645	2,230
Bala	500	0	1,543	64	38
Beypazarı	18,375	1,750	1,267	7,126	714
Elmadağ	1,649	-	1,101	1,150	400
Evren	200	-	485	293	120
Güdül	14,045	50	1,036	1,200	793
Haymana	5,040	-	407	96	103
Kahramankazan	8,910	104	5,685	660	426
Kalecik	4,317	78	11,302	21,677	1,389
Kızılcahamam	925	-	2,273	26	229
Nallıhan	7,800	430	757	600	271
Polatlı	6,316	96	2,030	87	1,204
Yenimahalle	75	-	97	21	20
Çamlıdere	72	-	314	11	92
Çubuk	13,260	110	898	271	7,347
Şereflikoçhisar	2,600	-	393	391	135
Total	128,287	3,627	39,658	35,170	17,821
Grand Total			**224,563**		

2.4.Calculation of Animal Waste Quantities and Energy Potential

Fertilizer production varies based on factors such as animal feeding density, nutrient types, and water intake (Hacısalihoğlu 2023; Kocabey 2019). This study utilized existing research on Ankara's biogas potential and applied literature-based assumptions summarized in Table 6 (Aktaş et al. 2015; Avcıoğlu et al. 2013). The total fresh manure amount (TFM) was calculated using Equation 1 as the product of animal weight (Wanimal) and species weight percentage (PWanimal). The usable fresh manure amount (TUFM) was then derived by applying the usability coefficient (UF) to TFM (Equation 2). Biogas calculations used dry manure estimates (TDMA) obtained via Equation 3, factoring in dry matter and volatile dry matter ratios. Biogas yields ranged from 200–350 m^3 per ton of dry manure for cattle, 100–310 m^3 for ovine animals, and 310–650 m^3 for poultry (Kurunç Sehan & Badem 2018).

Annual fresh manure potential (TFMP) was calculated using Equation 4, and biogas production (BAnnual) using Equation 5. With an assumed calorific value of 23.5 MJ/m^3, biogas energy potential (EBiogas) was determined via Equation 6, equating to 2.61 kWh/m^3 when accounting for 40% cogeneration efficiency. Additionally, CO_2 emissions prevented through biogas utilization were calculated using a 684 g/kWh coefficient, emphasizing its environmental benefits over coal combustion (Melikoglu 2013).

Table 6. Waste generation value ranges according to animal species.

Acceptance Parameters	Cattle	Ovine Animlas	Poultry
Animal weight (kg)	135-800	30-75	1.5-12
Fresh manure formation (%)	5-6	4-5	3-4
Fresh fertilizer production amount (kg/day)	6-48	1.2-3.75	0.45-0.48
Dry matter content (%)	5-25	30-36	10-90
Volatile dry matter (%)	75-85	20-81	60-80
Availability (%)	25-65	13	99
Biogas equivalence m^3/(ton*VDM)	200-350	100-310	310-650

Table 7. Acceptances used according to animal breeds.

Acceptance Parameters	Cattle	Ovine Animlas	Poultry
Total amount of fresh manure T_{FM} (kg/day)	27	2.48	0.26
Availability U_F (%)	65	13	99
The amount of biogas obtained from 1 ton of fresh manure depending on the animal species B_{FM} (m^3/ton)	33	58	78
Energy calorific value E_{biogas} (MJ/m^3)	23.5	23.5	23.5
Electrical energy value (kWh/year)	2.63	2.63	2.63
Prevented CO_2 emission value (g/kWh)	684	684	684

$$T_{FM} = W_{animal} \times PW_{animal} \quad \text{(Eq. 1)}$$

Where T_{FM} is total fresh manure amount (kg/day), W_{animal} is Weight by animal type (kg) and PW_{animal} is the percentage of weight of the animal by species (%).

$$T_{UFM} = T_{FM} \times U_F \quad \text{(Eq. 2)}$$

Where T_{UFM} is total usable fresh manure amount (kg/day) and U_F is usable fertilizer according to animal type (%). It is assumed as 65% for cattle, 13% for ovine animlas, and 99% for poultry.

$$T_{DMA} = T_{FM} \times DMRW_{animal} \times VDM_{animal} \quad \text{(Eq. 3)}$$

where T_{DMA} is total dry manure amount (ton*VDM/day), $DMRW_{animal}$ is the dry matter ratio in animal waste varies depending on the animal type (%). It ranges from 5-25% for cattle, 30% for ovine animlas, and 10-90% for poultry and VDM_{animal} is volatile dry matter ratio

according to animal type. Depending on the animal species, biogas generated from 1 ton of total dry manure varies between 200-300 m^3 (ton*VDM) for cattle, 100-350 m^3 (ton*VDM) for ovine animlas, and 310-650 m^3 (ton*VDM) for poultry (Kurunç Sehan and Badem 2018, Salihoğlu et al. 2019, Yağlı and Koç 2019).

$$T_{FMP} = T_{UFM} \times N_{animal} \times \frac{365}{1000} \quad \text{(Eq. 4)}$$

In this formula N_{animal} is represents the number of animals.

$$B_{Annual} = T_{FMP} \times B_{FM} \quad \text{(Eq. 5)}$$

where B_{Annual} is annual biogas production (m^3/year) and B_{FM} is the amount of biogas obtained from 1 ton of fresh manure depending on the animal species. It is assumed as 33 m^3/ton for cattle, 58 m^3/ton for ovine animlas, and 78 m^3/ton for poultry.

Biogas contains methane gas ranging from 50-70%. Therefore, the energy potential from biogas (E_{Biogas}):

$$E_{Biogas} = B_{Annual} \times B_{Calorific} \quad \text{(Eq. 6)}$$

where E_{Biogas} is represents the calorific value of energy produced annually (MJ/year) and $B_{Calorific}$ is represents the calorific value of biogas (MJ/m^3).

$$Electricity_{Biogas} = B_{Annual} \times 2.61\ kWh \quad \text{(Eq. 7)}$$

2.5.Calculation of Theoretical Biomass Potential from Agricultural Product Waste

The theoretical biomass potential from agricultural product waste has been calculated using the following equations (Tumen Ozdil and Caliskan 2022):

Theoretical biomass potential (TBP):

$$\mathrm{TBP} = \mathrm{CP} \times \mathrm{RPR} \times \left(\frac{100-\mathrm{M}}{100}\right) \quad \text{(Eq. 8)}$$

where CP is annual production quantity of the product in tons, RPR is ratio of product residue and M is moisture content of the product.

Theoretical energy potential (TEP):

$$\mathrm{TEP} = \mathrm{TBP} \times \mathrm{LHV} \quad \text{(Eq. 9)}$$

where LHV is Lower heating value.

Available energy potential (AEP):

$$\mathrm{AEP} = \mathrm{TEP} \times \mathrm{A} \quad \text{(Eq. 10)}$$

where A is availability factor.

Additionally, after calculating the available energy potential, the following formula is used to convert this energy into kWh (Özcan 2015):

$\mathrm{Electricity}_{\text{Biomass from Agricultural Waste}} = \mathrm{AEP} \times 0.277777778$ kWh (Eq. 11)

An emission factor of 230 gCO2/kWh is used in calculating the CO2 emissions that can be prevented annually by generating electricity from agricultural waste (Calculation Principles of CO2 Avoided Emissions Within EDF Group 2024).

The assumptions regarding annual production quantity, waste-product ratio, moisture content, and higher heating value for selected grains, fruits, and vegetables are provided in Table 8, based on assumptions made by reference.

Table 8. Product-waste ratio, moisture information, lower calorific value and usability values of selected grains, fruits and vegetables (Avcıoğlu et al. 2019, Karaca 2015, Tumen Ozdil and Caliskan 2022).

Herbal Product Type	Ratio of product residue (RPR)	Moisture (M) (%)	Availability (A) (%)	Lower heating value (LVH) (MJ/Ton)
Wheat	1.3	12.5	15	16,700
Barley	1.22	13	15	18,500
Sweetcorn (Maize)	1.88	16	60	17,000
Beans	1.45	5	15	14,700
Rye	0.99	15	15	17,400
Sugar beet	0.13	75	15	16,600
Sorghum	0.16	60	65	18,000
Chickpeas	0.67	69	70	18,000
Oat	0.84	70	59	18,000
Potatoes	0.45	60	90	13,700
Tomatoes	0.3	85	95	19,500
Cabbage	2.5	85	95	12,400
Apple	0.19	40	80	17,800
Grapes	0.42	45	80	18,000
Cherry	0.19	40	80	21,700

3. RESULTS AND DISCUSSIONS

3.1. Biogas Production Potential from Animal Waste

In order to determine the biogas potential from animal waste in Ankara, the number of animals and the total amount of wet waste that can be collected from these animals were calculated. First, the amount of wet manure

available for biogas production was determined, and then the biogas potential was calculated along with its thermal and electrical equivalents. Additionally, the reduction in CO_2 emissions resulting from the use of biogas energy, a renewable energy source, was calculated. Based on the total number of animals in Ankara in 2023 and certain assumptions, manure amounts, potential biogas production, energy potential, and the reduction in CO_2 emissions were determined.

In this study, for the year 2023, the numbers of cattle (local, culture, hybrid), small ruminants such as sheep and goats, and poultry including laying hens, turkeys, geese, ducks, and guinea fowl were provided based on TURKSTAT-TÜİK data (Table 1). Based on the number of animals across the province, the total wet manure potential was calculated using Equation 4 (Table 9) and the potential biogas production was calculated using Equation 5 (Table 10). Figure 5 shows the proportional distribution of biogas potential from animal waste by animal type across the districts of Ankara.

According to Table 9, the annual total available organic manure amount was calculated to be 5,495,000 tons, of which 71% is obtained from cattle, 4% from sheep and goats, and 25% from poultry. According to Table 10, the biogas energy potential for the entire province was determined to be 248,200,782 m^3/year. This energy potential consists of 52% from cattle, 5.2% from sheep and goats, and 42.8% from poultry. Figure 6 shows that the district with the highest animal-based biogas potential in Ankara is Polatlı.

After calculating the total annual biogas potential in Ankara, the thermal equivalent of the obtainable biogas was determined using Equation 6 (Table 11), and the electrical equivalents were calculated based on the assumptions provided in Table 6 and Equation 7 (Table 12). As a result of these calculations, the total annual electricity production potential from biogas in Ankara was determined to be 15,223,394,971 kWh (15,223,395 MWh). Figure 7 shows the map of the potential for electricity production from biogas obtained from animal waste in the districts of Ankara.

Table 9. Annual total fresh manure potential.

$T_{FMP} = T_{UFM} \times N_{animal} \times \frac{365}{1000}$ (Tonne/Year)				
District	**Cattle**	**Ovine Animlas**	**Poultry**	**Total**
Center	870,778	49,160	74,934	994,873
Akyurt	215,246	1,959	729	217,934
Ayaş	148,543	14,572	130,734	293,849
Bala	178,791	20,078	59,607	258,477
Beypazarı	91,698	11,419	149,334	252,451
Elmadağ	162,809	5,974	11,908	180,691
Evren	13,004	505	189	13,698
Güdül	80,789	9,029	26,942	116,760
Haymana	238,153	27,630	24,562	290,345
Kahramankazan	125,706	4,683	47,221	177,610
Kalecik	155,525	2,522	175,295	333,343
Kızılcahamam	159,913	6,194	17,188	183,295
Nallıhan	50,535	10,523	146,113	207,170
Polatlı	787,132	40,513	348,739	1,176,384
Yenimahalle	18,775	1,081	220	20,076
Çamlıdere	91,756	1,423	397	93,576
Çubuk	454,328	4,587	148,209	607,124
Şereflikoçhisar	67,318	9,308	718	77,344
Total	3,910,800	221,160	1,363,040	**5,495,000**

Table 10. Annual biogas production.

$B_{Annual} = T_{FMP} * B_{FM}$ (m3/Year)				
District	Cattle	Ovine Animlas	Poultry	Total
Center	28,735,688	2,851,285	5,844,860	37,431,833
Akyurt	7,103,118	113,640	56,830	7,273,588
Ayaş	4,901,917	845,159	10,197,284	15,944,360
Bala	5,900,099	1,164,551	4,649,363	11,714,013
Beypazarı	3,026,044	662,298	11,648,058	15,336,400
Elmadağ	5,372,682	346,482	928,847	6,648,010
Evren	429,121	29,294	14,766	473,181
Güdül	2,666,048	523,671	2,101,472	5,291,191
Haymana	7,859,048	1,602,538	1,915,820	11,377,407
Kahramankazan	4,148,312	271,602	3,683,245	8,103,160
Kalecik	5,132,332	146,285	13,673,039	18,951,656
Kızılcahamam	5,277,134	359,224	1,340,690	6,977,048
Nallıhan	1,667,654	610,317	11,396,797	13,674,768
Polatlı	25,975,361	2,349,762	27,201,625	55,526,748
Yenimahalle	619,583	62,683	17,148	699,414
Çamlıdere	3,027,947	82,558	30,962	3,141,466
Çubuk	14,992,818	266,053	11,560,311	26,819,182
Şereflikoçhisar	2,221,495	539,860	56,002	2,817,357
Total	129,056,402	12,827,262	106,317,118	**248,200,782**

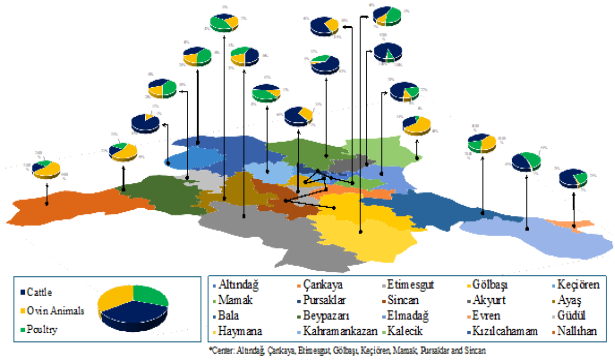

Figure 5. Proportional distribution of biogas potential resulting from animal waste in districts by animal type.

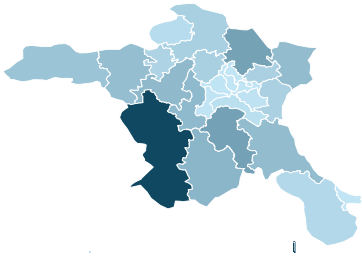

Figure 6. Biogas energy potential map resulting from animal waste in Ankara province by districts.

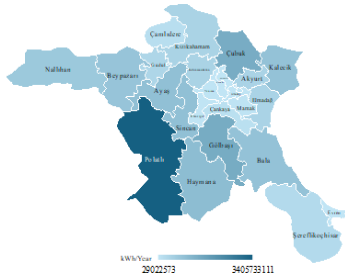

Figure 7. Electricity production potential from animal waste-derived biogas according to districts of Ankara province.

Table 11. Annual energy potential from biogas.

$E_{Biogas} = B_{Annual} * B_{Calorific}$ (MJ/Year)				
District	**Cattle**	**Ovine Animlas**	**Poultry**	**Total**
Center	675,288,678	67,005,203	137,354,198	879,648,080
Akyurt	166,923,282	2,670,533	1,335,505	170,929,321
Ayaş	115,195,047	19,861,229	239,636,180	374,692,457
Bala	138,652,334	27,366,951	109,260,020	275,279,305
Beypazarı	71,112,040	15,563,996	273,729,371	360,405,407
Elmadağ	126,258,024	8,142,320	21,827,894	156,228,238
Evren	10,084,348	688,404	347,008	11,119,760
Güdül	62,652,117	12,306,266	49,384,599	124,342,982
Haymana	184,687,631	37,659,652	45,021,775	267,369,058
Kahramankazan	97,485,343	6,382,655	86,556,254	190,424,252
Kalecik	120,609,796	3,437,690	321,316,419	445,363,905
Kızılcahamam	124,012,642	8,441,772	31,506,219	163,960,633
Nallıhan	391,898,63	14,342,448	267,824,731	321,357,042
Polatlı	610,420,986	55,219,410	639,238,191	1,304,878,587
Yenimahalle	14,560,209	1,473,044	402,977	16,436,229
Çamlıdere	71,156,749	1,940,106	727,596	73,824,452
Çubuk	352,331,223	6,252,256	271,667,302	630,250,781
Şereflikoçhisar	52,205,130	12,686,717	1,316,046	66,207,892
Total	3,032,825,443	301,440,652	2,498,452,284	**5,832,718,380**

Table 12. Annual electricity production potential from biogas.

$Electricity_{Biogas} = B_{Annual} * 2.61$ kWh (kWh/Year)				
District	**Cattle**	**Ovine Animlas**	**Poultry**	**kWh**
Center	1,762,503,451	174,883,580	358,494,458	2,295,881,489
Akyurt	435,669,766	6,970,092	3,485,669	446,125,527
Ayaş	300,659,074	51,837,808	625,450,430	977,947,312
Bala	361,882,591	71,427,743	285,168,651	718,478,985
Beypazarı	185,602,425	40,622,030	714,433,657	940,658,112
Elmadağ	329,533,443	21,251,454	56,970,804	407,755,701
Evren	26,320,148	1,796,735	905,690	29,022,573
Güdül	163,522,025	32,119,355	128,893,803	324,535,183
Haymana	482,034,717	98,291,690	117,506,834	697,833,241
Kahramankazan	254,436,744	16,658,729	225,911,823	497,007,296
Kalecik	314,791,567	8,972,371	838,635,853	1,162,399,791
Kızılcahamam	323,672,997	22,033,025	82,231,231	427,937,253
Nallıhan	102,285,542	37,433,789	699,022,549	838,741,880
Polatlı	1,593,198,772	144,122,661	1,668,411,678	3,405,733,111
Yenimahalle	38,002,145	3,844,644	1,051,769	42,898,558
Çamlıdere	185,719,116	5,063,678	1,899,027	192,681,820
Çubuk	919,584,493	16,318,387	70,9051,658	1,644,954,538
Şereflikoçhisar	136,255,389	33,112,332	3,434,879	172,802,599
Total	7,915,674,406	786,760,102	6,520,960,462	**15,223,394,971 (15,223,395 MWh)**

3.2.Biomass Energy Potential from Agricultural Waste

The total biomass energy potential from agricultural waste in Ankara is based on the agricultural production data provided in Tables 3, 4 and 5 the biomass energy calculations from agricultural waste presented in Table 8. These calculations determine the theoretical biomass energy potential (Equation 8), theoretical energy potential (Equation 9), usable energy potential (Equation 10), and electrical energy potential in kWh (Equation 11). Table 13 provides a detailed breakdown of these calculation results. According to Table 13, the annual total electrical energy that can be obtained from agricultural waste in Ankara is calculated to be 4,146,518,848 kWh (4,146,518 MW/year).

Table 13. Biomass energy potential from agricultural waste.

District	Annual Theoretical Biomass Potential $TBP = CP \times RPR \times \left(\frac{100 - M}{100}\right)$ (Tonne/Year)	Theoretical Energy Potential $TEP = TBP \times LHV$ (MJ/Year)	Available Energy Potential $AEP = TEP \times A$ (MJ/Year)	Electric $Electricity_{Biomass\ from\ Agricultural\ Waste} = AEP \times 0.277777778$ kWh (kWh/Year)
Center	452,148	7,843,394,602	2,023,471,067	556,049,842
Akyurt	41,226	714,441,813	172,855,265	47,748,993
Ayaş	337,370	5,806,332,396	2,537,545,447	699,103,320
Bala	242,888	4,235,039,039	1,138,522,629	311,148,307
Beypazarı	125,502	2,183,172,946	441,809,361	113,074,503
Elmadağ	46,693	819,232,283	134,850,931	61,447,015
Evren	27,906	486,941,800	84,849,340	22,711,088
Güdül	119,506	2,062,191,946	852,880,904	232,974,887
Haymana	352,524	6,127,408,313	1,332,459,435	354,704,203
Kahramankazan	85,819	1,476,561,841	564,214,980	152,590,203
Kalecik	120,211	2,066,081,696	728,390,528	178,168,939
Kızılcahamam	22,553	384,687,684	64,489,954	16,856,002
Nallıhan	84,541	1,462,968,384	418,767,340	117,728,153
Polatlı	677,812	11,572,616,150	3,200,648,152	882,937,765
Yenimahalle	8,038	138,128,313	21,568,837	6,118,842
Çamlıdere	1,621	28,414,428	7,438,492	1,524,475
Çubuk	62,671	1,093,199,299	297,133,214	81,908,335
Şereflikoçhisar	200,658	3,543,884,541	905,571,965	250,297,710
Total (Across Ankara Province)	**3,009,684 (Tonne Dry Mass)**	**52,044,697,473 (MJ/Year)**	**14,927,467,842 (MJ/Year)**	**4,146,518,848 kWh/Year (4,146,518 MWh/Year)**

3.3.Calculation of Prevented CO_2 Emissions Across the Province

Biogas generated from animal waste can prevent 684 g CO_2 per 1 kWh of electricity produced, while electricity generated from agricultural waste can prevent 230 g CO_2 per kWh. Based on the potential electricity generation from these sources, biogas from animal waste can prevent 10,412,802 tonnes of CO_2 emissions annually, and agricultural waste can prevent 940,031 tonnes of CO_2 emissions annually. The total CO_2 emissions reduction from both animal and agricultural biomass energy sources in Ankara is estimated at 11,352,833 tonnes (Table 14). This highlights the significant environmental benefits of clean

electricity production in reducing CO_2 emissions, a key contributor to global warming. Figure 2 illustrates the distribution of prevented CO_2 emissions by district, with the Polatlı district leading, contributing 22.3% of the total reduction (Figure 8).

Table 14. Annual prevented CO_2 emissions.

District	Preventing CO_2 Emission from Biomass Potential Sourced in Animal Waste $\frac{TonneCO_2 = Electricity_{Biogas} \times 684\ gCO_2}{1000000\ g/Tonne}$	Preventing CO_2 Emission from Biomass Potential Sourced in Agricultural Wastes $\frac{TonneCO_2 = Electricity_{Biomass\ from\ Agricultural\ Waste} \times 230\ gCO}{1000000\ g/Tonne}$	Annual Prevented CO_2 Emissions $TonneCO_2/Year$
Center	1,570,383	127,891	1,698,274
Akyurt	305,150	10,982	316,132
Ayaş	668,916	160,794	829,710
Bala	491,440	71,564	563,004
Beypazarı	643,410	26,007	669,417
Elmadağ	278,905	14,133	293,038
Evren	19,851	5,224	25,075
Güdül	221,982	53,584	275,566
Haymana	477,318	81,582	558,900
Kahramankazan	339,953	35,096	375,049
Kalecik	795,081	40,979	836,060
Kızılcahamam	292,709	3,877	296,586
Nallıhan	573,699	27,077	600,777
Polatlı	2,329,521	203,076	2,532,597
Yenimahalle	29,343	1,407	30,750
Çamlıdere	131,794	351	132,145
Çubuk	1,125,149	18,839	1,143,988
Şereflikoçhisar	118,197	57,568	175,765
Total	**10,412,802**	**940,031**	**11,352,833**

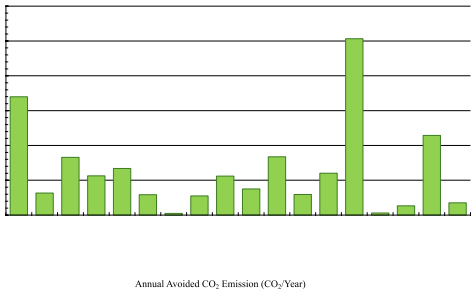

Figure 8. Distribution of annual prevented CO_2 emissions by districts of Ankara province.

In 2023, Ankara's total electricity consumption is estimated to be approximately 22,813,487 MWh, based on a population of 5,803,482 people and an annual per capita consumption of 3,931 kWh. The biomass energy potential

of Ankara shows that 19,369,913 MWh of electricity can be produced annually from animal and agricultural waste. This potential can meet 85% of the city's annual electricity demand, highlighting the significant role biomass energy can play as an environmentally friendly alternative energy source and its contribution to waste management.

4. CONCLUSION

This study determined the biomass energy potential from agricultural and livestock waste for Ankara province based on 2023 TÜİK data. It was calculated that 15,223,395 MWh of electricity can be produced annually from animal waste, while 4,146,518 MWh can be produced from selected agricultural waste. This energy offers considerable environmental benefits, as it is estimated to prevent 11,352,833 tons of CO_2 emissions annually, helping to mitigate climate change by reducing greenhouse gas emissions. Additionally, it decreases reliance on fossil fuels and promotes the use of renewable energy sources, addressing issues like air pollution and acid rain. Biomass energy also conserves natural resources, supports ecosystem sustainability, and enhances waste management efficiency by reducing pollution and minimizing land and disposal costs. Thus, biomass energy is crucial for environmental sustainability and provides eco-friendly energy alternatives. This energy can be utilized for electricity and heat production in various sectors, including residential, industrial, and agricultural applications, such as greenhouse heating. While studies on the energy potential from animal waste are common, research on

agricultural waste energy potential is less frequent. Converting agricultural residues into energy offers significant economic and energy security benefits, and assessing this potential based on regional climate conditions can substantially contribute to the regional economy and energy security.

REFERENCES

Adrese Dayalı Nüfus Kayıt Sistemi Sonuçları, 2023. (2024). Retrieved 5 July 2024, from https://data.tuik.gov.tr/

Aktaş, T., Özer, B., Soyak, G., & Ertürk, M. C. (2015). Tekirdağ İli'nde Hayvansal Atık Kaynaklı Biyogazdan Elektrik Üretim Potansiyelinin Belirlenmesi. Tarım Makinaları Bilimi Dergisi, 11(1), 69–74.

Ankara Coğrafyası. (n.d.). In Vikipedi. Vikipedi Özgür Ansiklopedi Org. Retrieved 4 July 2024 from https://tr.wikipedia.org/wiki/Ankara

Avcıoğlu, A. O., Çolak, A., & Türker, U. (2013). Türkiye'nin Tavuk Atıklarından Biyogaz Potansiyeli. Tekirdağ Ziraat Fakültesi Dergisi, 10(1), 21–28.

Avcıoğlu, A. O., Dayıoğlu, M. A., & Türker, U. (2019). Assessment of the Energy Potential of Agricultural Biomass Residues in Turkey. Renewable Energy, 138, 610–619.

Ayhan, A. (2015). Biogas Production Potential from Animal Manure of Bursa Province. Journal of Agricultural Faculty of Uludag University, 29(2), 47–53.

Baran, M. F., Lüle, F., & Gökdoğan, O. (2017). Adıyaman İlinin Hayvansal Atıklardan Elde Edilebilecek Enerji Potansiyeli. Türk Tarım ve Doğa Bilimleri Dergisi, 4(3), 245–249.

Bayrak Işık, E. H., & Polat, F. (2018). The Biogas Potential That Can Be Obtained From The Animal Wastes Of

Tokat Province. Gaziosmanpaşa Bilimsel Araştırma Dergisi, 7(3), 93–100.

Bharathiraja, B., Sudharsana, T., Jayamuthunagai, J., Praveenkumar, R., Chozhavendhan, S., & Iyyappan, J. (2018). Biogas production – A Review on Composition, Fuel Properties, Feed Stock and Principles of Anaerobic Digestion. Renewable and Sustainable Energy Reviews, 90, 570–582.

Biogas for Road Vehicles: Technology Brief. (2017). Retrieved 4 July 2024 from https://www.irena.org/

Bitkisel Üretim İstatistikleri. (2024). Retrieved 6 July 2024, from https://biruni.tuik.gov.tr/medas/?locale=tr

Bond, T., & Templeton, M. R. (2011). History and Future of Fomestic Biogas Plants in the Developing World. Energy for Sustainable Development, 15(4), 347–354. Retrieved from

Bulut, A. P., & Canbaz, G. T. (2019). Hayvan Atıklarından Sivas İli Biyogaz Potansiyelinin Araştırılması. Karaelmas Fen ve Mühendislik Dergisi, 9(1), 1–10.

Çağlayan, G., & Koçer, N. (2014). Muş İlinde Hayvan Potansiyelinin Değerlendirilerek Biyogaz Üretiminin Araştırılması. Muş Alparslan Üniversitesi Fen Bilimleri Dergisi, 2(1), 215–220.

Calculation Principles of CO2 Avoided Emissions Within EDF Group. (2024). EDF, 1–5. Retrieved 20 July 2024 from https://www.edf.fr/

Davenport, J., & Wayth, N. (2024). 2024 | 73'rd Edition Statistical Review of World Energy. Retrieved 4 July 2024 from London: https://www.energyinst.org/

Dhar, H., Kumar, S., & Kumar, R. (2017). A Review on Organic Waste to Energy Systems in India. Bioresource Technology, 245(Part A), 1229–1237.

Doruk, İ., & Bozdeveci, A. (2017). Denizli İlinin Kırsal Kesimlerinde Hayvansal Kaynaklı Atıklardan Biyogaz Potansiyelinin Belirlenmesi. Journal of the Institute of Science and Technology, 7(3), 181–186.

Flotats, X. (2019). Biogas: Perspectives of an Old Technology. In J. R. Bastidas Oyanedel & J. E. Schmidt (Eds.), Biorefinery (1st ed., pp. 313–349). Cham: Springer.

Fulghum, N. (2024). Yearly Electricity Data (2024). Retrieved 4 July 2024 from https://ember-energy.org/

Genel Coğrafya ve Yeryüzü Şekilleri. (n.d.). Retrieved 4 July 2024, from http://www.ankara.gov.tr/

Hacısalihoğlu, S. (2023). Hayvansal Atıkların Yönetimi, Bursa-Karacabey Örneği. Balıkesir Üniversitesi Fen Bilimleri Enstitüsü Dergisi, 25(2), 403–415.

Hayvancılık İstatistikleri. (2024). Retrieved 5 July 2024 from https://biruni.tuik.gov.tr/

Holdren, J. P. (1991). Population and The Energy Problem. Population and Environment, 12(3), 231–255.

Işık, S., & Yavuz, S. (2022). Investigation of Biogas Production Potential from Livestock Manure by

Anaerobic Digestion in Bingöl Province. Türk Doğa ve Fen Dergisi, 11(1), 116–122.

Karaca, C. (2015). Mapping of Energy Potential Through Annual Crop Residues in Turkey. International Journal of Agricultural an Biological Engineering IJABE, 8(2), 104–109.

Kaya, D., & Öztürk, H. (2012). Biyogaz Teknolojisi: Üretim-Kullanım-Projeleme (1st ed.). Kocaeli: Umuttepe Yayınları.

Koç, E., & Kaya, K. (2015). Enerji Kaynakları-Yenilenebilir Enerji Durumu. Mühendis ve Makina, 56(668), 36–47.

Kocabey, S. (2019). Balıkesir İli İçin Hayvansal Atık Kaynaklı Biyogaz Potansiyelinin Belirlenmesi. European Journal of Science and Technology, (17), 234–243.

Koçer, N. N., Öner, C., & Sugözü, İ. (2006). Türkiye'de Hayvancılık Potansiyeli ve Biyogaz Üretimi. Fırat Üniversitesi Doğu Araştırmaları Dergisi, 4(2), 17–20.

Kurunç Sehan, A., & Badem, A. (2018). Erzincan İlindeki Hayvansal Atıkların Biyogaz Potansiyelinin Araştırılması. Academic Platform-Journal of Engineering and Science, 6(1), 25–35.

Li, Y., Alaimo, C. P., Kim, M., Kado, N. Y., Peppers, J., Xue, J., … Kleeman, M. J. (2019). Composition and Toxicity of Biogas Produced from Different Feedstocks in California. Environmental Science & Technology, 53(19), 11569–11579.

Melikoglu, M. (2013). Vision 2023: Feasibility analysis of Turkey's renewable energy projection. Renewable Energy, 50, 570–575.

Omer, A. M., & Fadalla, Y. (2003). Biogas Energy Technology in Sudan. Renewable Energy, 28(3), 499–507.

Özcan, O. (2015). Photovoltaic System Application for Eskişehir's Light Rail Transporting System (EsTram). Eruopean Solar Prize.

Reay, D., Smith, P., & Amstel, A. van (Eds.). (2010). Methane Sources and the Global Methane Budget. London & Washington: Earthscan Publishing for a Sustainable Future.

Robles, G., Nair, R. B., Kleinsteuber, S., Nikolausz, M., & Sárvári Horváth, I. (2018). Biogas Production: Microbiological Aspects. In M. Tabatabaei & H. Ghanavati (Eds.), Biogas (1st ed., pp. 163–198). Cham: Springer.

Salihoğlu, N. K., Teksoy, A., & Altan, K. (2019). Büyükbaş ve Küçükbaş Hayvan Atıklarından Biyogaz Üretim Potansiyelinin Belirlenmesi: Balıkesir İli Örneği. Ömer Halisdemir Üniversitesi Mühendislik Bilimleri Dergisi, 8(1), 3147.

Share of Electricity Generation From Fossil Fuels, Renewables and Nuclear, Turkey. (2024). Retrieved 4 July 2024, from https://ourworldindata.org/

Share of Electricity Generation From Fossil Fuels, Renewables and Nuclear, World. (2024). Retrieved 4 July 2024, from https://ourworldindata.org/

Tumen Ozdil, N. F., & Caliskan, M. (2022). Energy Potential from Biomass from Agricultural Crops: Development Prospects of the Turkish Bioeconomy. Energy, 249, 123770.

Taşkesen, E., Acar, Ş., Ertuğrul, G., Arlı, F., Dumrul, H., & Bulbul, S. (2022). Şırnak-Uludere bölgesinde yaygın olarak bulunan asfaltitlerden doğal hümik asit elde edilebilirliğinin incelenmesi. Politeknik Dergisi, 25(2), 691-697.

Vijin Prabhu, A., Sivaram, A. R., Prabhu, N., & Sundaramahalingam, A. (2021). A Study of Enhancing The Biogas Production in Anaerobic Digestion. Materials Today: Proceedings, 45(Part 9), 7994–7999.

Yağlı, H., & Koç, Y. (2019). Hayvan Gübresinden Biyogaz Üretim Potansiyelinin Belirlenmesi: Adana İli Örnek Hesaplama. Çukurova Üniversitesi Mühendislik-Mimarlık Fakültesi Dergisi, 34(3), 35–48.

A DECISION SUPPORT FRAMEWORK FOR MATERIAL COMBINATION SELECTION IN THE FURNITURE INDUSTRY[1]

Hilal SİNGER[2]

Abdullah Cemil İLÇE[3]

1. INTRODUCTION

The furniture industry is a dynamic sector that continually evolves to meet the changing preferences and needs of consumers. Over the years, it has seen significant transformations driven by advancements in design, materials, and manufacturing technologies. From traditional wooden furniture to modern, sleek designs using metal and glass, the industry has embraced a wide range of materials to enhance durability, aesthetics, and functionality. Sustainability has also become a crucial consideration, prompting manufacturers to seek eco-friendly alternatives that reduce environmental impact while maintaining high-quality standards (Azizi et al.,

[1] This study is based on the experimental data of the project supported by the Düzce University Scientific Research Projects Coordination (Project No: BAP- 2009.03.01.036), conducted under the supervision of the second author.

[2] Dr. Res. Asst., Bolu Abant Izzet Baysal University, Faculty of Engineering, Department of Industrial Engineering, e-mail: hilal.singer@ibu.edu.tr, ORCID: 0000-0003-0884-2555.

[3] Assoc. Prof. Dr. Bolu Abant Izzet Baysal University, Faculty of Engineering, Department of Industrial Engineering, e-mail: cemililce@ibu.edu.tr, ORCID: 0000-0001-5133-683X.

2016; Muhammad Suandi et al., 2022). Wood-plastic composites (WPCs) have emerged as a revolutionary material in the furniture industry. These composites offer a unique combination of the natural look of wood and the durability of plastic. WPCs are highly valued for their resistance to moisture, decay, and insect damage, making them an ideal choice for both indoor and outdoor furniture. WPCs present an eco-friendly alternative to traditional wood (Mitaľová et al., 2024).

Material combination selection is an important aspect in the development and optimization of WPCs, directly influencing their performance and suitability for various applications. Selecting the appropriate combination of different materials is significant for achieving the desired balance of properties such as strength, durability, and aesthetic appeal (Leu et al., 2012). To navigate these complex decisions, the multicriteria decision-making (MCDM) technique can be used by decision-makers. MCDM provides a structured framework for evaluating multiple conflicting criteria, allowing for a more informed and balanced selection of alternatives. This approach ensures that all relevant aspects are considered, leading to optimized results that meet the diverse needs of consumers and industries alike (Mehdi et al., 2012).

The selection of material combinations is a multifaceted decision that requires careful consideration of various criteria. Given the diverse nature of these criteria, their importance varies based on the specific application. Weighting methods in MCDM help prioritize these criteria based on their importance. It is essential to prioritize them

appropriately (Singer & İlçe, 2024). To achieve this, a linear programming method to generate weights in the analytic hierarchy process (LP-GW-AHP) can be used. The LP-GW-AHP method combines the strengths of linear programming and the AHP method to derive weights for decision elements. This method aims to optimize the accuracy of the weight derivation process by formulating it as a linear programming problem. The LP-GW-AHP method involves pairwise comparisons of decision elements to assess their relative importance. Decision-makers compare each pair of elements to create pairwise comparison matrices. These comparisons are usually done using a 1-9 scale. The traditional AHP method involves normalization steps for pairwise comparison matrices. In contrast, the LP-GW-AHP method simplifies this process by directly formulating and solving a single linear programming model based on decision-makers' evaluations. The LP-GW-AHP method enhances the traditional AHP by reducing computational complexity (Hosseinian et al., 2012). This method has been successfully employed by several researchers (Gotzamani et al., 2018; Kamvysi et al., 2014; Mendoza Mendoza et al., 2016; Şengül et al., 2016).

Once the weights of decision criteria are determined, alternatives can be analyzed via various MCDM methods. MCDM facilitates a comprehensive assessment of different alternatives by considering multiple criteria simultaneously (Emovon & Oghenenyerovwho, 2020). The additive ratio assessment system (ARAS) method is one of the most popular MCDM methods designed to evaluate and rank a set of alternatives based on multiple criteria.

This method involves five steps: forming a decision matrix, normalizing data, obtaining a normalized weighted matrix, determining optimality functions and utility degrees, and prioritization (Liu & Xu, 2021). The ARAS method has been effectively used to solve many decision problems in the literature (Bahrami et al., 2019; Ghenai et al., 2020; Karabašević et al., 2018; Zavadskas et al., 2010).

The present study focuses on the material combination selection problem in the furniture industry. This study utilizes the LP-GW-AHP method to determine criteria weights and the ARAS method to rank alternatives. Once the importance of each criterion is determined using the LP-GW-AHP procedure, the ARAS procedure is employed to analyze and rank different material combinations. The study presents its novelty by applying the LP-GW-AHP and ARAS methods to this field.

2. LP-GW-AHP/ARAS APPROACH

The current study proposes a LP-GW-AHP/ARAS approach for selecting the best material combination in the furniture industry. This approach consists of two main phases: (i) evaluating decision criteria and (ii) prioritizing material combinations. The steps of this approach are detailed below (Hosseinian et al., 2012; Yıldırım, 2015).

Step 1: Define the decision problem and create a hierarchical model with the goal, criteria, and alternatives.

Step 2: Perform pairwise comparisons of criteria using the 1-9 AHP scale. These comparisons are used to construct a pairwise comparison matrix where each

element a_{ij} represents the relative importance of element i to element j.

$$M = [1\ a_{12}\ \dots\ a_{1n}\ a_{21}\ 1\ \dots\ a_{2n}\ \vdots\ \vdots\ \ddots \\ \vdots\ a_{n1}\ a_{n2}\ \dots\ 1\ ]_{n\times n};\ a_{ij} > 0, a_{ij} = \frac{1}{a_{ji}} \quad (1)$$

Step 3: Calculate a consistency ratio (CR) to ensure the comparisons are consistent. If the CR is above 0.1, the comparisons need to be reviewed and adjusted.

$$CR = \frac{(\frac{\lambda_{max} - n}{n-1})}{RC} \quad (2)$$

Here, λ_{max} is the maximum eigenvalue of matrix M and the RC is obtained from the Saaty index table (Saaty, 1977).

Step 4: Formulate a mathematical model as described below.

$$Max\ Z \quad (3)$$

subject to:

$$w_i \geq Z \qquad i = 1, \dots, n \quad (4)$$

$$\sum_{j=1}^{n} a_{ij} v_j - w_i = 0 \qquad i = 1, \dots, n \quad (5)$$

$$\sum_{i=1}^{n} w_i = 1 \quad (6)$$

$$v_i - \frac{1}{\beta} w_i \geq 0 \qquad i = 1, \dots, n \qquad (7)$$

$$v_i - \frac{1}{n} w_i \leq 0 \qquad i = 1, \dots, n \qquad (8)$$

$$w_i \geq 0;\ v_i \geq 0 \qquad i = 1, \dots, n \qquad (9)$$

Here, w_i represents weights for criteria and v_j denotes output weights produced by the model. The following formula is employed to obtain the β parameter:

$$\beta = min\left\{\left(\frac{1}{r_i}\sum_{j=1}^{n} \quad a_{ij} r_j\right), \left(\frac{1}{c_i}\sum_{j=1}^{n} \quad a_{ij} c_j\right)\right\} \qquad (10)$$

Here, r_i and c_i denote the row and column sums of matrix M, respectively.

Step 5: Solve the formulated model to calculate the weight of each criterion.

Step 6: Construct a decision matrix for alternatives.

$$X = \begin{bmatrix} x_{01} & \cdots & x_{0j} & \cdots & x_{0n} \\ \vdots & \ddots & \vdots & \ddots & \vdots \\ x_{i1} & \cdots & x_{ij} & \cdots & x_{in} \\ \vdots & \ddots & \vdots & \ddots & \vdots \\ x_{m1} & \cdots & x_{mj} & \cdots & x_{mn} \end{bmatrix} \qquad (11)$$

The matrix $X = [x_{ij}]$ contains the performance scores of alternative i with respect to criterion j. The first row consists of the best (ideal) solutions.

Step 7: Normalize the constructed matrix to eliminate the influence of different measurement units and make criteria comparable.

For benefit criteria:

$$\underline{x}_{ij} = \frac{x_{ij}}{\sum_{i=0}^{m} x_{ij}} \quad (12)$$

For cost criteria:

$$x_{ij}^{*} = \frac{1}{x_{ij}} \quad (13)$$

$$\underline{x}_{ij} = \frac{x_{ij}^{*}}{\sum_{i=0}^{m} x_{ij}^{*}} \quad (14)$$

Step 8: Calculate the weighted normalized decision matrix.

$$\hat{x}_{ij} = \underline{x}_{ij}.w_j \quad (15)$$

Step 9: Determine optimality functions (S_i) and utility degrees (K_i).

$$S_i = \sum_{j=1}^{n} \hat{x}_{ij} \quad (16)$$

$$K_i = \frac{S_i}{S_0} \quad (17)$$

Step 10: Rank alternatives based on their utility degrees. The alternative with the highest score is considered the best option.

3. APPLICATION

This study conducts a multicriteria decision analysis on various properties of five composite materials made from eastern beech (*Fagus Orientalis* L.) and polycarbonate boards, with a focus on their suitability for furniture production. The data acquisition process for the alternatives is briefly outlined as follows. First, the preparatory procedures are completed. The materials are sanded to a thickness of 4 mm using 100 grit sandpaper. The samples are conditioned at 20±2°C and 65±5% relative humidity. Composite materials are produced using beech veneer panels (A) and polycarbonate boards (B) in several configurations: ABABA, ABBBA, and AABAA, bonded with polyurethane adhesives. Additionally, ABTBA and ATBTA configurations (where T represents a polycarbonate board placed perpendicular to the fibers) are included in the experimental design. The samples are stored in a climate chamber at 20±2°C and 65±5% relative humidity until their weights stabilize.

A two-phase decision-making approach is proposed to select the most suitable material combination in the furniture industry. Initially, the LP-GW-AHP method is utilized to determine the weights of various criteria. Once these weights are identified, the ARAS method is applied to evaluate different material combinations. This process is visualized in Figure 1.

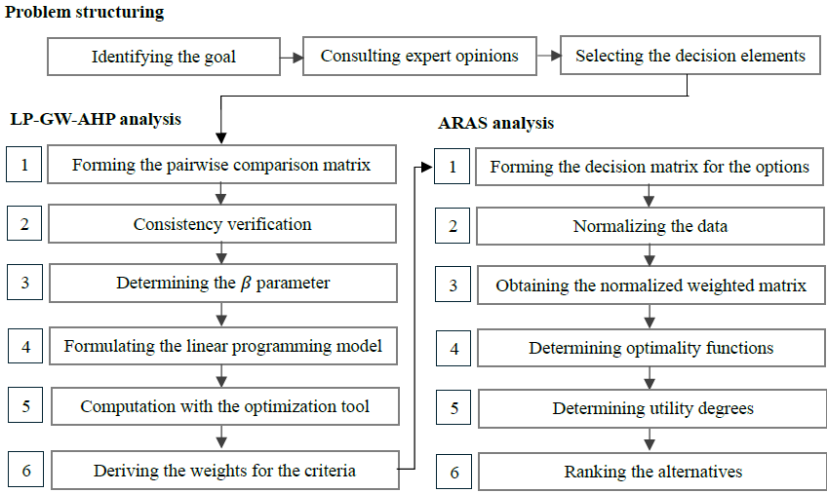

Figure 1. Decision-making framework

After consulting expert opinions and reviewing relevant literature, the criteria for material combination selection are determined as moisture content [%], thickness swelling - 2h [%], water absorption - 2h [%], specific gravity [g/cm^3], modulus of elasticity [N/mm^2], and bending strength [N/mm^2]. The alternative material combinations under consideration are ABABA, ABBBA, AABAA, ABTBA, and ATBTA. The decision elements are presented in Figure 2.

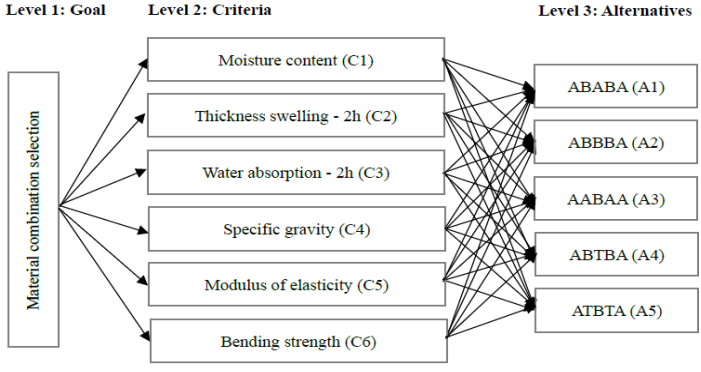

Figure 2. Hierarchical structure of the decision problem

A decision-making team is formed to analyze the criteria. The experts in the team are industrial and woodworking industrial engineers. These experts are selected based on their experience, knowledge, and articles related to the research topic. The experts are asked to compare the criteria in pairs using Table 1 (Ramezanpour et al., 2015). These comparisons are used to create the pairwise comparison matrix, which can be seen in Table 2.

Table 1. AHP scale

Numerical rating	Degree of importance
1	Equally important
3	Moderately important
5	Strongly important
7	Very strongly important
9	Extremely important
2, 4, 6, and 8	For compromise between the above values

Table 2. Pairwise comparison matrix for the criteria

Criterion	C1	C2	C3	C4	C5	C6
C1	1	2	2	1/4	1/3	1/4
C2		1	1	1/5	1/4	1/5
C3			1	1/5	1/4	1/5
C4				1	2	1/2
C5					1	1/2
C6						1

CR = 0.02

The β parameter is determined by applying Equation (10) to the pairwise comparison matrix. The results of this calculation process are given in Table 3. After obtaining the β value, a mathematical model is established based on the experts' evaluations. This model is coded in GAMS 24.1.3 optimization software. After the formulated model is run,

the weight of each criterion is obtained. The modeling results for the criteria are presented in Table 4.

Table 3. β calculation

#	r_i	$\sum_{j=1}^{n} a_{ij} r_j$	$\frac{1}{r_i}\sum_{j=1}^{n} a_{ij}$	#	c_i	$\sum_{j=1}^{n} a_{ij} c_j$	$\frac{1}{c_i}\sum_{j=1}^{n} a_{ij}$
1	5.833	31.892	5.467	1	13.000	75.700	5.823
2	3.150	19.767	6.275	2	18.000	119.333	6.630
3	3.150	19.767	6.275	3	18.000	119.333	6.630
4	17.500	107.833	6.162	4	4.150	22.817	5.498
5	13.000	73.950	5.688	5	5.833	32.767	5.617
6	19.000	134.833	7.096	6	2.650	18.092	6.827
max			7.096	max			6.827
β = 6.827							

Table 4. Modeling results for the criteria

Criteria	Weight	Ranking
Moisture content (C1)	0.083	4
Thickness swelling - 2h (C2)	0.052	5
Water absorption - 2h (C3)	0.052	5
Specific gravity (C4)	0.274	2
Modulus of elasticity (C5)	0.190	3
Bending strength (C6)	0.349	1

The modeling results indicate that bending strength (weight: 0.349) is the most important criterion. Specific gravity holds significant influence with a weight of 0.274, placing it second. Modulus of elasticity is ranked third with a weight of 0.190. Moisture content, with a weight of 0.083, ranks fourth. Both thickness swelling and water absorption, each with a weight of 0.052, are the least important criteria, sharing the fifth rank.

After calculating the weights of the criteria, the ARAS method is applied to evaluate the performances of

the alternatives based on the criteria. The decision matrix used in the ARAS analysis is presented in Table 5. The decision matrix, created according to the experimental results, is first normalized and then weighted. The optimality functions and utility degrees are determined sequentially to prioritize the alternatives. The ARAS results are presented in Table 6.

Table 5. Decision matrix for the alternatives

Element	C1	C2	C3	C4	C5	C6
A0	5.19	0.29	0.55	0.38	8548.92	59.24
A1	6.56	0.38	0.87	0.46	6870.50	43.92
A2	5.66	0.29	0.56	0.39	5418.92	31.53
A3	8.52	0.42	1.14	0.60	8548.92	59.24
A4	5.31	0.33	0.55	0.38	1539.50	24.12
A5	5.19	0.31	0.58	0.38	1019.08	20.54

Table 6. ARAS results

Element	S_i	K_i	$\%K_i$	Ranking
A0	0.224			
A1	0.173	0.7739	77.39	2
A2	0.162	0.7241	72.41	3
A3	0.191	0.8537	85.37	1
A4	0.129	0.5771	57.71	4
A5	0.121	0.5425	54.25	5

The ranking result obtained for the alternatives indicates that a layered material combination of AABAA is identified as the most suitable for furniture production. The material sequence starts with two layers of eastern beech, followed by a single layer of polycarbonate, and ends with another two layers of eastern beech. AABAA offers the optimal balance of the factors for high-quality and attractive furniture production.

4. CONCLUSION

The furniture industry consistently evolves to align with the shifting preferences and needs of consumers. One of the critical aspects of this adaptation is the selection of material combinations. In this context, the selection of material combinations plays an important role in the development and optimization of WPCs. These selections directly impact the performance and applicability of WPCs across various furniture production scenarios. This study focuses on evaluating five composite materials made from eastern beech (*Fagus Orientalis* L.) and polycarbonate boards for furniture production using a decision-making approach.

The study utilizes a two-phase methodology to identify the most suitable material combination in the furniture industry. Initially, the LP-GW-AHP method is employed to ascertain the weights of different criteria. Following this, the ARAS method is used to evaluate and rank the material combinations based on these criteria. According to the results, bending strength is the most important criterion, followed by specific gravity and modulus of elasticity. Furthermore, the material combination labeled AABAA (A: eastern beech, B: polycarbonate) is found to be the most suitable for furniture production.

This study underscores the importance of a systematic approach in selecting material combinations for composites. By prioritizing key performance metrics and employing effective analytical methods, manufacturers can enhance the quality and suitability of their products,

ultimately better meeting consumer demands and advancing industry standards. In future studies, the number of material combinations can be increased, different decision elements can be included in the problem, and different decision support tools can be applied to solve the problem.

REFERENCES

Azizi, M., Mohebbi, N., & De Felice, F. (2016). Evaluation of sustainable development of wooden furniture industry using multi criteria decision making method. *Agriculture and Agricultural Science Procedia*, *8*, 387–394. doi: 10.1016/j.aaspro.2016.02.034

Bahrami, Y., Hassani, H., & Maghsoudi, A. (2019). BWM-ARAS: A new hybrid MCDM method for Cu prospectivity mapping in the Abhar area, NW Iran. *Spatial Statistics*, *33*, 100382. doi:10.1016/j.spasta.2019.100382

Emovon, I., & Oghenenyerovwho, O. S. (2020). Application of MCDM method in material selection for optimal design: A review. *Results in Materials*, *7*, 100115. doi:10.1016/j.rinma.2020.100115

Ghenai, C., Albawab, M., & Bettayeb, M. (2020). Sustainability indicators for renewable energy systems using multi-criteria decision-making model and extended SWARA/ARAS hybrid method. *Renewable Energy*, *146*, 580–597. doi:10.1016/j.renene.2019.06.157

Gotzamani, K., Georgiou, A., Andronikidis, A., & Kamvysi, K. (2018). Introducing multivariate Markov modeling within QFD to anticipate future customer preferences in product design. *International Journal of Quality & Reliability Management*, *35*(3), 762–778. doi:10.1108/IJQRM-11-2016-0205

Hosseinian, S. S., Navidi, H., & Hajfathaliha, A. (2012). A new linear programming method for weights

generation and group decision making in the analytic hierarchy process. *Group Decision and Negotiation*, *21*(3), 233–254. doi:10.1007/s10726-009-9182-x

Kamvysi, K., Gotzamani, K., Andronikidis, A., & Georgiou, A. C. (2014). Capturing and prioritizing students' requirements for course design by embedding Fuzzy-AHP and linear programming in QFD. *European Journal of Operational Research*, *237*(3), 1083–1094. doi:10.1016/j.ejor.2014.02.042

Karabašević, D., Maksimović, M., Stanujkić, D., Jocić, G., & Rajčević, D. (2018). Selection of software testing method by using ARAS method. *Tehnika*, *73*(5), 724–729. doi:10.5937/tehnika1805724K

Leu, S.-Y., Yang, T.-H., Lo, S.-F., & Yang, T.-H. (2012). Optimized material composition to improve the physical and mechanical properties of extruded wood–plastic composites (WPCs). *Construction and Building Materials*, *29*, 120–127. doi:10.1016/j.conbuildmat.2011.09.013

Liu, N., & Xu, Z. (2021). An overview of ARAS method: Theory development, application extension, and future challenge. *International Journal of Intelligent Systems*, *36*(7), 3524–3565. doi:10.1002/int.22425

Mehdi, Z., Mohammad, H. A., Nahid, R., & Sarfaraz, H. Z. (2012). A hybrid fuzzy multiple criteria decision making (MCDM) approach to combination of materials selection. African *Journal of Business*

Management, *6*(45), 11171–11178. doi:10.5897/AJBM11.2022

Mendoza Mendoza, A. A., Ospino Castro, W. A., & Romero Martinez, D. S. (2016). Applying LP-GW-AHP decision-making methods and fuzzy logic to select an elective course in the University of the Atlántico, Colombia. *Revista Virtual Universidad Católica Del Norte*, *48*, 351–364.

Mitaľová, Z., Mitaľ, D., & Berladir, K. (2024). A concise review of the components and properties of wood–plastic composites. *Polymers*, *16*(11), 1556. doi: 10.3390/polym16111556

Muhammad Suandi, M. E., Amlus, M. H., Hemdi, A. R., Abd Rahim, S. Z., Ghazali, M. F., & Rahim, N. L. (2022). A review on sustainability characteristics development for wooden furniture design. *Sustainability*, *14*(14), 8748. doi:10.3390/su14148748

Ramezanpour, B., Pronker, E. S., Kreijtz, J. H. C. M., Osterhaus, A. D. M. E., & Claassen, E. (2015). Market implementation of the MVA platform for pre-pandemic and pandemic influenza vaccines: A quantitative key opinion leader analysis. *Vaccine*, *33*(35), 4349–4358. doi:10.1016/j.vaccine.2015.04.086

Saaty, T. L. (1977). A scaling method for priorities in hierarchical structures. *Journal of Mathematical Psychology*, *15*(3), 234–281. doi:10.1016/0022-2496(77)90033-5

Şengül, Ü., Eren, M., & Shiraz, S. E. (2016). Application of linear programming to derive the local weight in the

analytic hierarchy process. *International Journal of Operational Research*, *27*(3), 450–468. doi:10.1504/IJOR.2016.078937

Singer, H., & İlçe, A. C. (2024). Mobilya üretiminde malzeme kombinasyonu seçimi için çok kriterli bir çözüm yaklaşımı. *Gazi Üniversitesi Fen Bilimleri Dergisi Part C: Tasarım ve Teknoloji*, *12*(1), 117–127. doi:10.29109/gujsc.1397494

Yıldırım, B. F. (2015). Çok kriterli karar verme problemlerinde ARAS yöntemi. *Kafkas Üniversitesi İktisadi ve İdari Bilimler Fakültesi*, *6*(9), 285–296.

Zavadskas, E. K., Turskis, Z., & Vilutiene, T. (2010). Multiple criteria analysis of foundation instalment alternatives by applying Additive Ratio Assessment (ARAS) method. *Archives of Civil and Mechanical Engineering*, *10*(3), 123–141. doi:10.1016/S1644-9665(12)60141-1

GRAPHENE-BASED NANOFLUIDS IN PV/T SYSTEMS

Hakan DUMRUL[1]

Fatih ARLI[2]

Edip TAŞKESEN[3]

Serdal DAMARSEÇKİN[4]

Hüseyin GÜRBÜZ[5]

1. INTRODUCTION

With technological advancements and industrialization, the increasing needs in people's lives and the growth in population are leading to a rise in energy demand and installed capacity in countries. Most of the energy produced on Earth comes from fossil fuel sources. Due to the negative effects of fossil fuel sources (greenhouse gas emissions, global warming) and their limited availability, the use of renewable energy sources in energy production has increased (Celik & Özgür, 2020; Lamb et al., 2021). Due to its zero greenhouse gas

[1] Assistant Professor, Şırnak University, Faculty of Engineering, Energy Systems Engineering, hakandumrul@sirnak.edu.tr, ORCID: 0000-0003-1122-3886.

[2] Assistant Professor, Şırnak University, Faculty of Engineering, Energy Systems Engineering, fatiharli@sirnak.edu.tr, ORCID: 0000-0002-0899-3460.

[3] Assistant Professor, Şırnak University, Faculty of Engineering, Energy Systems Engineering edip.taskesen@sirnak.edu.tr, ORCID: 0000-0002-3052-9883.

[4] Assistant Professor, Şırnak University, Faculty of Engineering, Energy Systems Engineering, serdalseckin@hotmail.com, ORCID: 0000-0003-4427-6220.

[5] Assoc. Prof. Dr., Şırnak University, Faculty of Engineering, Mechanical Engineering, huseyinngurbuz@gmail.com, ORCID: 0000-0002-3561-7786.

emissions, inexhaustible solar energy stands as an indispensable renewable energy source. For the effective and efficient use of such an important resource, scientists conduct a significant number of studies and publish numerous articles (Kabir, Kumar, Kumar, Adelodun, & Kim, 2018; Makarieva, Gorshkov, & Li, 2008; Prăvălie, Patriche, & Bandoc, 2019; Siow, Lee, Ooi, & Von Lau, 2024). As proof of the conducted studies, articles related to solar energy in the literature can be provided in Figure 1.

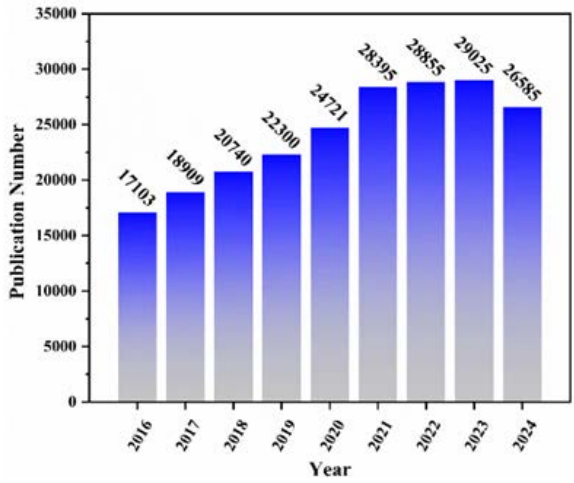

Figure 1. Web of Science "solar energy" keyword publication statistics (document type review or research article).

Photovoltaic (PV) modules absorb the rays in the visible spectrum from solar radiation and generate electrical energy through the photovoltaic effect (Oh, Bae, Chae, Jeong, & Nam, 2023). Photovoltaic modules convert approximately 20% of solar energy into electrical energy, depending on ambient temperature, dust accumulation, shading, wind speed, irradiation, and module surface temperature, while the other portion of the energy is released as heat energy, causing an increase in module

surface temperature (Al-Ezzi & Ansari, 2022; Fayaz, Nasrin, Rahim, & Hasanuzzaman, 2018; Hussain, Batra, & Pachauri, 2017; Mustafa, Gomaa, Al-Dhaifallah, & Rezk, 2020; Sheikholeslami, Khalili, & Mousavi, 2023; Zhao, Hu, Ao, Xuan, & Pei, 2020). This increase in temperature on the surface of PV modules causes a decrease in electrical power or efficiency, and this decrease varies by 1-2% at temperatures above 30 ^{o}C (Kazem, 2019). Therefore, it is very important to increase the efficiency and electrical power output of PV modules by removing the heat generated in their thermal management. In the literature, many techniques have been developed and applied to cool PV modules (Figure 2). Depending on environmental conditions, etc., it is very important to determine which technique will be used for temperature management of PV modules (Gharzi, Arabhosseini, Gholami, & Rahmati, 2020).

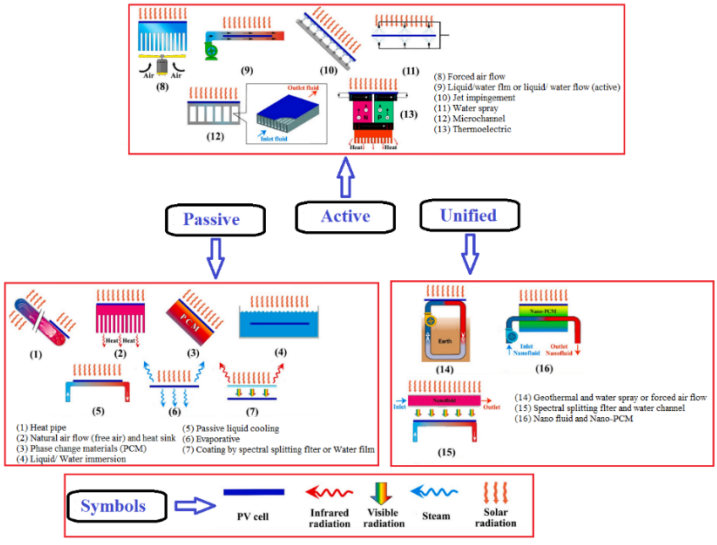

Figure 2. Schematic classification of PV cooling techniques (Gharzi et al., 2020).

In the cooling techniques presented in Figure 2, it is stated by scientists in recent studies that nanofluids with higher heat transfer properties compared to basic fluids (air, water, ethylene glycol, etc.) with low thermal conductivity are used as heat transfer fluids, and thus the performance of PV modules is further increased (Ahmed, Ahshan, Mondal, & Hossain, 2021; Gupta & Pradhan, 2021; Hajjaj, Aqeel, Sultan, Shahar, & Shah, 2022; Kandeal et al., 2021). When examining nanofluids formed as stable suspensions by simply dispersing nanoparticles with high thermal conductivity in a base fluid for PV applications; nanofluids obtained from graphene, which have higher thermal conductivity and more advanced thermophysical properties compared to commonly used metal oxide nanofluids such as Al_2O_3, CuO, TiO_2, ZnO, and SiO_2, and metal nanofluids composed of Cu, Au, Ag, and Al, make graphene nanofluids more attractive for heat removal from PV modules (Angayarkanni & Philip, 2015; Arshad, Jabbal, Yan, & Reay, 2019; Borode, Ahmed, & Olubambi, 2019; Huang et al., 2021; Safiei, Rahman, Yusoff, & Radin, 2020). After Novoselov and Geim successfully isolated graphene in 2004, graphene-based nanofluids have been used in many cooling applications to enhance heat transfer, one of which is photovoltaic thermal (PV/T) technology. To maximize PV efficiency, graphene-based nanofluids are being studied in PV/T systems to reduce module surface temperatures (Lee, Hwang, & Lee, 2019). To obtain high-efficiency electrical and thermal energy from solar energy, the optimization of nanofluids and the selection of suitable fluids as cooling mediums in PV/T collectors are highly attracting researchers (Rafaizul et al., 2024).

This chapter focuses on the impact of graphene-based nanofluids on the performance of PV/T systems. The section has been structured into a total of five sections, emphasizing the importance of graphene-based nanofluids in the cooling of solar energy and PV modules. In the second section, comprehensive information about PV/T collectors is presented, and the factors affecting their performance are discussed. In section 3, the properties, application areas, and graphene-based nanofluids have been discussed. Section 4 emphasizes the effect of graphene-based nanofluids on the performance of PV/T collectors. Section 5 concludes with the evaluation of the results.

2. PV/T SYSTEMS

In PV modules, an increase in temperature has a negative impact on electrical efficiency and power output (Manikandan et al., 2022). Therefore, the fundamental method in studies on PV/T technology is the cooling of PV surfaces (Kazem, 2019). PV/T collectors are systems where PV modules are combined with thermal absorbers to contribute to energy conversion performance through cooling (Salameh, Tawalbeh, Juaidi, Abdallah, & Hamid, 2021). To enable PV modules to operate at the desired temperature, increase the overall efficiency of the PV system, reduce the installation area and cost, utilize the heat extracted from the modules in low or medium temperature applications in industrial or residential areas, and to make sufficient use of solar energy, PV/T systems have been developed (Fayaz, Rahim, Hasanuzzaman,

Nasrin, & Rivai, 2019; Yazdanifard, Ameri, & Ebrahimnia-Bajestan, 2017). Figure 3 shows a typical PV/T system configuration. When considering the overall efficiency in PV/T systems, they are more advantageous compared to PVs (Abbas et al., 2019; Al-Waeli, Kazem, Chaichan, & Sopian, 2021).

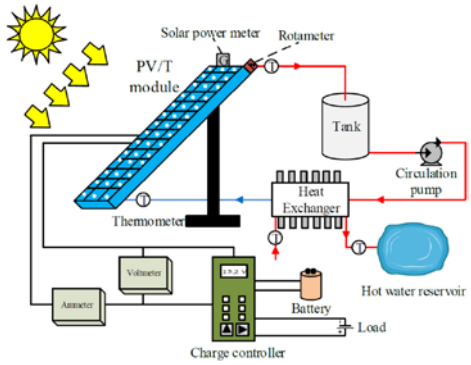

Figure 3. PV/T system diagram (Abbas et al., 2019).

In improving the performance of PV/T systems and determining the installation of these systems, climate, design, and operational parameters are considered. As climate variables, solar radiation, relative humidity, wind speed, ambient temperature, and accumulated dust can be considered; as design variables, solar tracking systems, pipe/channel collector depth, collector tilt angle, PV module type, glass thickness and type, absorber sheet material type, pipe radius and thickness, and thermal insulation can be given; and finally, as operational variables, the working fluid, fluid flow rate, type of working fluid, and packing factor can be provided (Elbreki et al., 2016; Yandri, 2019). PV/T systems can generally be classified based on heat extraction, operating environment,

applications, and whether they have concentrators, and a broad classification of PV/Ts is provided in Figure 4.

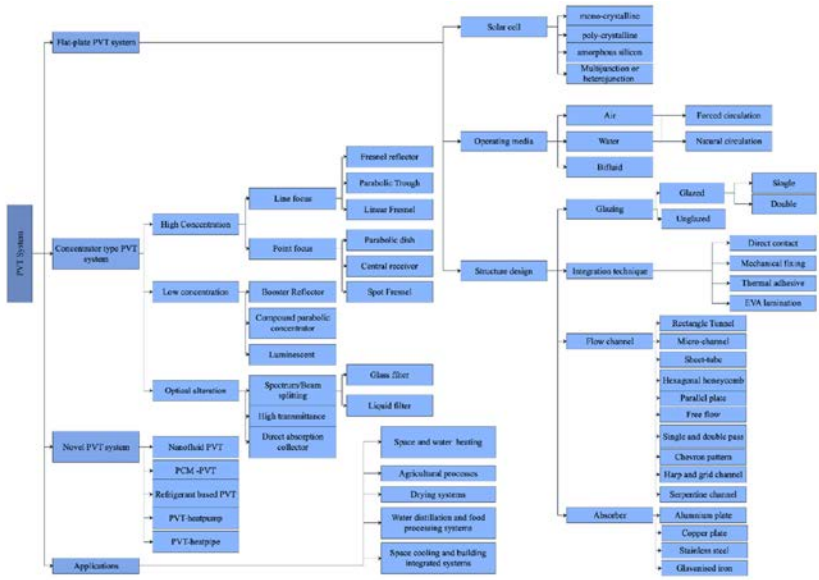

Figure 4. PV/T system classification (Bandaru et al., 2021).

As seen in the classification of PV/T systems, many system designs are carried out theoretically, simulated, or experimentally. The performance analysis of these systems is conducted using the first and second laws of thermodynamics. The first law of thermodynamics is the law of conservation of energy and is only concerned with the amount of energy. Generally, the first law is considered in system energy analysis (Dincer & Cengel, 2001; Joshi, Dincer, & Reddy, 2009; Salari, Taheri, Farzanehnia, Passandideh-fard, & Sardarabadi, 2021; Sansaniwal, Sharma, & Mathur, 2018). In the design and analysis of solar energy systems, both mass and energy conservation principles can be applied together in exergy calculations. Exergy analysis provides both a quantitative and

qualitative analysis of energy. Exergy analysis is based on the second law of thermodynamics, which requires the calculation of the total exergy input, exergy output, and the exergy destroyed (Dubey, Solanki, & Tiwari, 2009; Joshi et al., 2009; Sansaniwal et al., 2018). In Table 1, the energy and exergy equations used for PV/T systems are expressed.

Table 1. Summary of general equation expressions used in PV/T systems.

Ref.	Eq.	Statement	Explanation
Sardarabadi et al., 2014	$\dot{E}_{m,i} + \dot{E}_s = \dot{E}_l + \dot{E}_e + \dot{E}_{m,o}$	Enerji dengesi	The general energy balance equation for quasi-steady-state processes
Jasim et al., 2022	$\dot{E}x_s + \dot{E}x_{m,i} = \dot{E}x_e + \dot{E}x_{m,o} + \dot{E}x_{dest}$	Ekserji dengesi	The general exergy balance equation for quasi-steady-state processes
Jasim et al., 2022	$\dot{E}_s = GA_{si}$	Solar energy	G is the solar intensity. A_{si} is solar imposed surface area.
Jakhar et al., 2017	$\dot{E}x_s = \dot{E}_s\left(1 - \frac{4}{3}\frac{T_a}{T_{sun}} + \frac{1}{3}\left(\frac{T_a}{T_{sun}}\right)^4\right)$	Solar exergy	T_{sun} is the temperature of the sun, T_a is the ambient temperature.
Sardarabadi et al., 2014	$\dot{E}_e = V_{oc}I_{sc}FF$	Electrical power	V_{oc} is open-circuit voltage. I_{sc} is short circuit current.
Kazemian et al., 2018a,b	$\dot{E}_{th} = \dot{m}c_{p,f}\left(T_{f,o} - T_{f,i}\right)$	Thermal power	$\dot{m}$ is the mass flow rate of circulated fluid in the system, $c_{p,f}$ is the specifc heat capacity of the fluid, $T_{f,i}$ and $T_{f,o}$ are the inlet and outlet fluid temperatures.
Mahdavi et al., 2019	$\eta_e = \frac{\dot{E}_e}{\dot{E}_s} = \frac{VI}{GA_{si}}$	Electrical efficiency	
Salem Ahmed et al., 2019	$\eta_{th} = \frac{\dot{Q}_{th}}{\dot{E}_s} = \frac{\dot{m}c_{p,f}\left(T_{f,o} - T_{f,i}\right)_{PV/T}}{GA_{si}}$	Thermal efficiency	
Jasim et al., 2022	$\dot{E}x_e = \dot{E}_e$	Electrical exergy	
Kazemian et al., 2018a,b	$\dot{E}x_{th} = c_{p,f}\left[\left(T_{f,o} - T_{f,i}\right) - \left(T_a \ln\left(\frac{T_{f,o}}{T_{f,i}}\right)\right)\right] - \frac{\Delta P_f}{\rho}$	Thermal exergy	
Jasim et al., 2022	$\eta_{II} = \frac{\dot{E}x_e + \dot{E}x_{th}}{\dot{E}x_s}$	Exergy efficiency	

3. NANOFLUIDS: GRAPHENE-BASED NANOFLUIDS

3.1.Nanofluids

The increase in energy demand, the depletion of fossil fuel sources, and the problems arising from the use of these fuels, as well as the need to leave a liveable environment for future generations, necessitate finding alternative sources for these energy sources (renewable energy sources; solar, wind, geothermal, hydrogen, biomass, etc.) or maximizing energy efficiency in technologies that work with fossil fuel sources (Khare, Nema, & Baredar, 2016; Ladjevardi, Asnaghi, Izadkhast, & Kashani, 2013; Pordanjani et al., 2021; Saidur, Meng, Said, Hasanuzzaman, & Kamyar, 2012). Nanotechnology, due to its beneficial effects, can be used in various processes of energy production through different technologies by many scientific fields, minimizing losses in energy efficiency values (Behera, Sangwai, & Byun, 2025; Benelmekki, 2015). By utilizing the superior physical, chemical, optical, and thermal properties of nanoparticles used in nanotechnology compared to other similar materials in bulk form, desired targets in energy efficiency are achieved in various fields such as energy production, energy transport, and energy storage. The areas where nanotechnology is used are shown in Figure 5 (B. A. Bhanvase, Barai, Sonawane, Kumar, & Sonawane, 2018; B. Bhanvase & Barai, 2021).

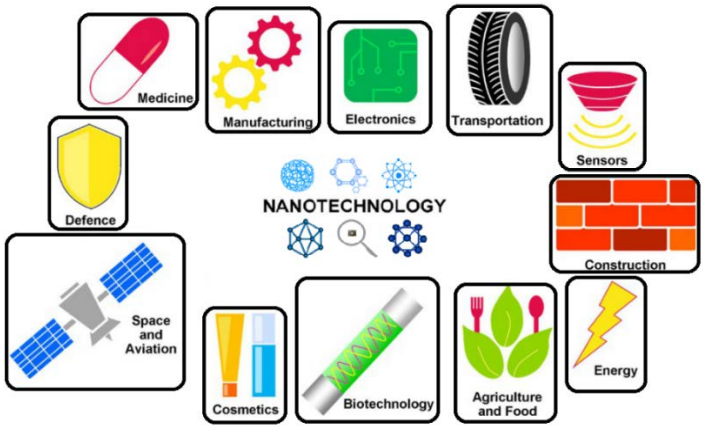

Figure 5. Different nanotechnology application areas (B. Bhanvase & Barai, 2021).

The foundation of nanotechnology is formed by nanoparticles and the nanofluids prepared from them. In the production of nanofluids that provide superior thermophysical properties to the base fluids, two different methods are used: top-down and bottom-up (B. A. Bhanvase et al., 2018; Chamsa-Ard, Brundavanam, Fung, Fawcett, & Poinern, 2017). In these two methods, the material size is prepared from small to large or from large to small using physical, chemical, biological, and physicochemical methods (B. Bhanvase & Barai, 2021; Pordanjani et al., 2021; Taylor et al., 2013). The term nanofluid, first used by Stephen Choi in 1995, is defined as a mixture in which nanoparticles (1-100 nm) are added and suspended in a base fluid (water, ethylene glycol, propylene glycol, alcohol, etc.) (Ghadimi, Saidur, & Metselaar, 2011; Pang, Lee, & Kang, 2015). In the determination of the base fluid in nanofluids, factors such as viscosity, heat capacity and stability, freezing-boiling point, non-reactivity with nanoparticles, non-

encouragement of agglomeration, and non-corrosiveness are taken into consideration (Akilu, Baheta, Said, Minea, & Sharma, 2018; Tembhare, Barai, & Bhanvase, 2022). The production processes of nanofluids are carried out using two methods: single-phase and two-phase. In the more stable and non-agglomerating single-step method, the distribution of nanoparticles in the base fluid is achieved in a single stage. This method is not commonly preferred due to its high cost, low production of nanofluids, and the formation of unwanted products during the preparation stage as a result of the reagents reacting with each other. The two-step method also allows to produce a large amount of nanofluid at a low cost, but it has issues such as stability and agglomeration. To overcome these problems, the pH of the suspension is usually changed, ultrasonic treatment is applied, or surfactants are used (Devendiran & Amirtham, 2016; Kiani, Meshksar, Makarem, & Rahimpour, 2022). The choice between these two methods is made based on the targeted application, cost, and production scale. The stability of nanofluids is directly related to particle size, agglomeration, base fluid properties, base fluid and nanoparticle interaction, sedimentation, and zeta potential, and is especially indirectly related to thermal conductivity, density, specific heat, viscosity, friction factor, pressure drop, and surface tension (B. Bhanvase & Barai, 2021). Nanofluids are classified according to the nanoparticles they are produced from, as shown in Figure 6 (Mehta, Subhedar, Panchal, & Said, 2022).

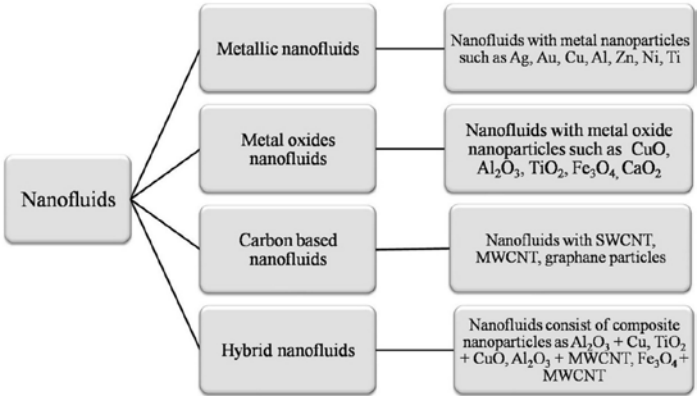

Figure 6. Nanofluid classification (Awais et al., 2021; Mehta et al., 2022).

Nanofluids offer superior thermophysical properties compared to base fluids (such as water, oil, or ethylene glycol). These properties make nanofluids highly attractive for heat transfer applications. In particular, the increase in thermal conductivity, viscosity changes, density, specific heat capacity, and thermal stability are among the key factors affecting the performance of nanofluids. Figure 7 presents a summary of the key parameters (e.g., nanoparticle concentration, particle size and shape, fluid flow regime, temperature) that determine the heat transfer performance of nanofluids and the thermal properties of nanofluids. These parameters and properties provide a general framework for how nanofluids can be optimized in specific applications (Bellos, Said, & Tzivanidis, 2018; Timofeeva, 2011).

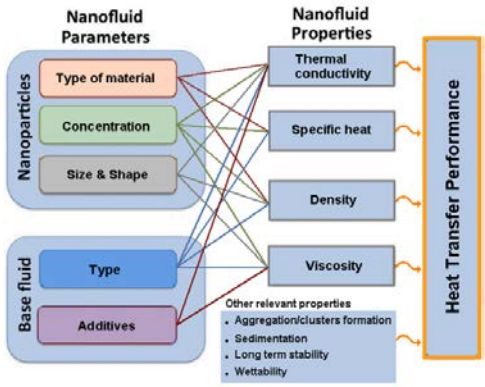

Figure 7. Nanofluid properties that affect heat transfer efficiency (Souza et al., 2022).

3.2.Graphene-Based Nanofluids

Graphene was first identified by Benjamin Collins Brodie in 1859 and later theoretically studied by Wallace (Dasari Shareena, McShan, Dasmahapatra, & Tchounwou, 2018). Although it was first imaged with an electron microscope in 1962, a significant milestone in understanding the properties of graphene was achieved in 2004 when Andre Geim and Konstantin Novoselov isolated a single atom-thick layer of graphene from bulk graphite (Shams, Zhang, & Zhu, 2015; Shinohara & Tiwari, 2015; Trivedi, Lobo, & Matte, 2019). This study led to the discovery of graphene's unique chemical, mechanical, optical, physical, electrical, and thermal properties, earning these scientists the Nobel Prize in 2010 (Bharech & Kumar, 2015; Enoki & Ando, 2019). Today, graphene nanoparticles and their derivatives, such as graphene oxide (GrO) and reduced graphene oxide (rGrO), graphene nanoplatelets, and nanoparticles, are used in various applications in many fields (purification, energy storage, biosensors, solar cells, transistors, heat transfer, etc.) (Bahiraei & Heshmatian,

2019; Liu, Xue, Zhang, & Dai, 2012; Mbayachi, Ndayiragije, Sammani, Taj, & Mbuta, 2021). Graphene, a two-dimensional carbon allotrope with a honeycomb structure, can be produced through various chemical, electrochemical, and mechanical processes. According to the nanofluid preparation techniques mentioned in Section 3.1, graphene-based nanofluids can be prepared, but it is observed that the two-step method is used in most scientific studies. In this method, hydrophobic graphene is mixed with hydrophilic surfactants to achieve a homogeneous distribution in water or other base fluids, reducing agglomeration (Arshad et al., 2019; Bahiraei & Heshmatian, 2019; Elsaid et al., 2021; Rasheed, Khalid, Rashmi, Gupta, & Chan, 2016; Sadeghinezhad et al., 2016). Graphene-based nanofluids have a wide range of thermal conductivity (6–5,000 W/m.K) and are therefore preferred as an effective heat transfer fluid in heat transfer studies. However, due to the high density and viscosity of graphene-based nanofluids, they require higher pressure drop and pumping power. This negative effect can be eliminated through optimization in volumetric fractioning (Elsaid et al., 2021). Graphene-based nanofluids stand out in heat transfer applications due to their superior thermophysical properties; however, disadvantages such as cost, stability, difficulties in achieving homogeneous distribution, and increases in density and viscosity limit their broader applicability in heat transfer studies.

4. THE EFFECT OF GRAPHENE-BASED NANOFLUIDS ON PV/T PERFORMANCE

Due to the excellent thermal, electrical, and optical properties of graphene and graphene-derived nanoparticles used in the preparation of graphene-based nanofluids, they have been preferred by scientists in recent years for selective spectral separation in the cooling of PV modules or as working fluids in heat transfer applications. Graphene-based nanofluids, despite having disadvantages such as high cost, stability, viscosity, and density, are used in PV/T systems due to their higher thermal conductivity compared to other types of nanofluids, providing significant improvements in the power outputs, thermal and electrical efficiencies, heat transfer properties, and exergies of these systems (Hamzat, Omisanya, Sahin, Oyetunji, & Olaitan, 2022; Huq, Ong, Chew, Leong, & Kazi, 2022; Rafaizul et al., 2024; Salari et al., 2021; Siow et al., 2024; Vaka, Walvekar, Rasheed, Khalid, & Panchal, 2019). In the literature, the effects of graphene-based nanofluids' superior thermophysical properties on PV/T performance are being studied. Venkatesh et al., 2022, in their experimental study, stated that when a 0.3 vol % graphene nanoplatelet (GnP)/H_2O mixture was used, the PV module temperature decreased from 60 ^oC to 45 ^oC, and the PV/T system efficiency increased by 13%. Alshikhi & Kayfeci, 2022, in their experimental studies, compared the effects of aluminium oxide (Al_2O_3), Hybrid, and GnP nanofluids on PV/T performance at a flow rate of 0.5 l/min and a concentration of 0.5 wt% to water. They determined that the best increase in the total energy efficiency of the PV/T system was 56.1% with GnP/H_2O. Alous et al., 2019,

experimentally investigated the effects of multi-walled carbon nanotube (MWCNT)/H_2O and GnP/H_2O nanofluids on the performance of the PV/T system at a flow rate of 0.5 l/min and a concentration of 0.5 wt%. As a result, they stated that the exergy efficiencies were 12.1% for the MWCNT/H_2O nanofluid and 20.6% for the GnP/H_2O nanofluid. Alwan Sywan Alshaheen et al., 2020, in their study found that with a GnP/H_2O nanofluid concentration of 0.05 wt% and an optimal flow rate of 50 kg/h, the total energy efficiency of the PV/T system was 19.3% for GnP/H_2O, 15.24% for single-walled carbon nanotube SWCNT/H_2O, and 9.46% for MWCNT/H_2O compared to pure water. They stated that the GnP/H_2O nanofluid better improved the PV/T performance. Taheri et al., 2021, in their experimental study, examined the change in PV/T performance when the concentrations of deionized H_2O, GnP/H_2O, SWCNT/H_2O, and MWCNT/H_2O nanofluids were 0.05 wt% and the fluid flow rate was 50 kg/h. As a result, when evaluating the exergy efficiencies, they explained that the highest efficiency increases of 2.32% belonged to GnP/H_2O. When studies on the performance of PV/T systems are examined, it is observed that graphene-based nanofluids significantly increase system efficiency and more than meet the expected performance in system improvements. The superior thermal conductivity and heat transfer properties of these nanofluids enable the optimization of thermal, electrical, and overall efficiency in PV/T systems.

5. CONCLUSION

In this section, the importance and applications of solar energy, cooling techniques for PV modules, nanofluids as heat transfer fluids and their properties, PV/T systems, and experimental studies on the performance of graphene-based PV/T systems are discussed. Solar energy is gaining increasing importance worldwide as one of the environmentally friendly and sustainable energy sources. In this context, the development of cooling techniques to enhance the efficiency of PV modules is of great importance. Nanofluids offer a promising solution in this field due to their high thermal conductivity and heat transfer capacities. Graphene-based nanofluids possess superior thermophysical properties, and the improvements they provide in enhancing heat transfer, thermal, electrical, and overall efficiency in experimental studies related to performance enhancement in PV/T systems are quite remarkable. However, in heat transfer studies, it should also be considered that factors such as the homogeneous distribution of graphene nanoparticles within the base fluid, the stability of graphene-based nanofluids, cost, and performance optimization need to be considered. In conclusion, graphene-based nanofluids stand out as an important innovative component with the potential to enhance the performance of PV/T systems. However, to ensure the broader applicability of these technologies, further research is needed on factors such as economic efficiency and long-term stability. These studies will enable significant steps to be taken towards increasing the

efficiency of solar energy systems and producing environmentally friendly energy solutions.

Acknowledgments

The authors show their gratitude to Şırnak University's Coordinatorship of Scientific Research Projects (CRP) for providing financial support by project number 2023.FNAP.06.03.02.

REFERENCES

Abbas, N., Awan, M. B., Amer, M., Ammar, S. M., Sajjad, U., Ali, H. M., … Jafry, A. T. (2019). Applications of nanofluids in photovoltaic thermal systems: a review of recent advances. *Physica A: Statistical Mechanics and Its Applications*, 536, 122513.

Ahmed, S., Ahshan, K. H. N., Mondal, M. N. A., & Hossain, S. (2021). Application of metal oxides-based nanofluids in PV/T systems: a review. *Frontiers in Energy*, 1–32.

Akilu, S., Baheta, A. T., Said, M. A. M., Minea, A. A., & Sharma, K. V. (2018). Properties of glycerol and ethylene glycol mixture based SiO2-CuO/C hybrid nanofluid for enhanced solar energy transport. *Solar Energy Materials and Solar Cells*, 179, 118–128.

Al-Ezzi, A. S., & Ansari, M. N. M. (2022). Photovoltaic solar cells: a review. *Applied System Innovation*, 5(4), 67.

Al-Waeli, A. H. A., Kazem, H. A., Chaichan, M. T., & Sopian, K. (2021). A review of photovoltaic thermal systems: Achievements and applications. *International Journal of Energy Research*, 45(2), 1269–1308.

Alous, S., Kayfeci, M., & Uysal, A. (2019). Experimental investigations of using MWCNTs and graphene nanoplatelets water-based nanofluids as coolants in PVT systems. *Applied Thermal Engineering*, 162(August), 114265.

Alshikhi, O., & Kayfeci, M. (2022). Experimental investigation of using graphene nanoplatelets and

hybrid nanofluid as coolant in photovoltaic thermal systems. *Thermal Science*, 26(1 Part A), 195–208.

Alwan Sywan Alshaheen, A., Kianifar, A., & Baradaran Rahimi, A. (2020). Experimental study of using nano-(GNP, MWCNT, and SWCNT)/water to investigate the performance of a PVT module: Energy and exergy analysis. *Journal of Thermal Analysis and Calorimetry*, 139, 3549–3561.

Angayarkanni, S. A., & Philip, J. (2015). Review on thermal properties of nanofluids: Recent developments. *Advances in Colloid and Interface Science*, 225, 146–176.

Arshad, A., Jabbal, M., Yan, Y., & Reay, D. (2019). A review on graphene based nanofluids: Preparation, characterization and applications. *Journal of Molecular Liquids*, 279, 444–484.

Awais, M., Ullah, N., Ahmad, J., Sikandar, F., Ehsan, M. M., Salehin, S., & Bhuiyan, A. A. (2021). Heat transfer and pressure drop performance of Nanofluid: A state-of-the-art review. *International Journal of Thermofluids*, 9, 100065.

Bahiraei, M., & Heshmatian, S. (2019). Graphene family nanofluids: A critical review and future research directions. *Energy Conversion and Management*, 196, 1222–1256.

Bandaru, S. H., Becerra, V., Khanna, S., Radulovic, J., Hutchinson, D., & Khusainov, R. (2021). A review of photovoltaic thermal (PVT) technology for residential applications: performance indicators, progress, and opportunities. *Energies*, 14(13), 3853.

Behera, U. S., Sangwai, J. S., & Byun, H.-S. (2025). A comprehensive review on the recent advances in applications of nanofluids for effective utilization of renewable energy. *Renewable and Sustainable Energy Reviews*, 207, 114901.

Bellos, E., Said, Z., & Tzivanidis, C. (2018). The use of nanofluids in solar concentrating technologies: a comprehensive review. *Journal of Cleaner Production*, 196, 84–99.

Benelmekki, M. (2015). An introduction to nanoparticles and nanotechnology. *Designing Hybrid Nanoparticles*, 1–14.

Bhanvase, B. A., Barai, D. P., Sonawane, S. H., Kumar, N., & Sonawane, S. S. (2018). Intensified heat transfer rate with the use of nanofluids. In *Handbook of nanomaterials for industrial applications* (pp. 739–750). Elsevier.

Bhanvase, B., & Barai, D. (2021). *Nanofluids for heat and mass transfer: Fundamentals, sustainable manufacturing and applications*. Academic Press.

Bharech, S., & Kumar, R. (2015). A review on the properties and applications of graphene. *J. Mater. Sci. Mech. Eng*, 2(2025), 70–73.

Borode, A., Ahmed, N., & Olubambi, P. (2019). A review of solar collectors using carbon-based nanofluids. *Journal of Cleaner Production*, 241, 118311.

Celik, A. N., & Özgür, E. (2020). Review of Turkey's photovoltaic energy status: Legal structure, existing installed power and comparative analysis. *Renewable*

and Sustainable Energy Reviews, 134.

Chamsa-Ard, W., Brundavanam, S., Fung, C. C., Fawcett, D., & Poinern, G. (2017). Nanofluid types, their synthesis, properties and incorporation in direct solar thermal collectors: A review. *Nanomaterials*, 7(6), 131.

Dasari Shareena, T. P., McShan, D., Dasmahapatra, A. K., & Tchounwou, P. B. (2018). A review on graphene-based nanomaterials in biomedical applications and risks in environment and health. *Nano-Micro Letters*, 10, 1–34.

Devendiran, D. K., & Amirtham, V. A. (2016). A review on preparation, characterization, properties and applications of nanofluids. *Renewable and Sustainable Energy Reviews*, 60, 21–40.

Dincer, I., & Cengel, Y. A. (2001). *Energy, entropy and exergy concepts and their roles in thermal engineering*. *Entropy* (Vol. 3).

Dubey, S., Solanki, S. C., & Tiwari, A. (2009). Energy and exergy analysis of PV/T air collectors connected in series. *Energy and Buildings*, 41(8), 863–870.

Elbreki, A. M., Alghoul, M. A., Al-Shamani, A. N., Ammar, A. A., Yegani, B., Aboghrara, A. M., … Sopian, K. (2016). The role of climatic-design-operational parameters on combined PV/T collector performance: A critical review. *Renewable and Sustainable Energy Reviews*, 57, 602–647.

Elsaid, K., Abdelkareem, M. A., Maghrabie, H. M., Sayed, E. T., Wilberforce, T., Baroutaji, A., & Olabi, A. G.

(2021). Thermophysical properties of graphene-based nanofluids. *International Journal of Thermofluids*, 10, 100073.

Enoki, T., & Ando, T. (2019). *Physics and chemistry of graphene: graphene to nanographene*. CRC Press.

Fayaz, H., Nasrin, R., Rahim, N. A., & Hasanuzzaman, M. (2018). Energy and exergy analysis of the PVT system: Effect of nanofluid flow rate. *Solar Energy*, 169(November 2017), 217–230.

Fayaz, H., Rahim, N. A., Hasanuzzaman, M., Nasrin, R., & Rivai, A. (2019). Numerical and experimental investigation of the effect of operating conditions on performance of PVT and PVT-PCM. *Renewable Energy*, 143, 827–841.

Ghadimi, A., Saidur, R., & Metselaar, H. S. C. (2011). A review of nanofluid stability properties and characterization in stationary conditions. *International Journal of Heat and Mass Transfer*, 54(17–18), 4051–4068.

Gharzi, M., Arabhosseini, A., Gholami, Z., & Rahmati, M. H. (2020). Progressive cooling technologies of photovoltaic and concentrated photovoltaic modules: A review of fundamentals, thermal aspects, nanotechnology utilization and enhancing performance. *Solar Energy*, 211(July), 117–146.

Gupta, S. K., & Pradhan, S. (2021). A review of recent advances and the role of nanofluid in solar photovoltaic thermal (PV/T) system. *Materials Today: Proceedings*, 44, 782–791.

Hajjaj, S. S. H., Aqeel, A. A. K. A., Sultan, M. T. H., Shahar, F. S., & Shah, A. U. M. (2022). Review of recent efforts in cooling photovoltaic panels (PVs) for enhanced performance and better impact on the environment. *Nanomaterials*, 12(10), 1664.

Hamzat, A. K., Omisanya, M. I., Sahin, A. Z., Oyetunji, O. R., & Olaitan, N. A. (2022). Application of nanofluid in solar energy harvesting devices: A comprehensive review. *Energy Conversion and Management*, 266, 115790.

Huang, P., Li, Y., Yang, G., Li, Z.-X., Li, Y.-Q., Hu, N., … Novoselov, K. S. (2021). Graphene film for thermal management: A review. *Nano Materials Science*, 3(1), 1–16.

Huq, T., Ong, H. C., Chew, B. T., Leong, K. Y., & Kazi, S. N. (2022). Review on aqueous graphene nanoplatelet nanofluids: preparation, stability, thermophysical properties, and applications in heat exchangers and solar thermal collectors. *Applied Thermal Engineering*, 210, 118342.

Hussain, A., Batra, A., & Pachauri, R. (2017). An experimental study on effect of dust on power loss in solar photovoltaic module. *Renewables: Wind, Water, and Solar*, 4, 1–13.

Jakhar, S., Soni, M. S., & Gakkhar, N. (2017). An integrated photovoltaic thermal solar (IPVTS) system with earth water heat exchanger cooling: Energy and exergy analysis. *Solar Energy*, 157, 81–93.

Jasim, O. M. J., Selimli, S., Dumrul, H., & Yilmaz, S. (2022).

Closed-loop aluminium oxide nanofluid cooled photovoltaic thermal collector energy and exergy analysis, an experimental study. *Journal of Energy Storage*, 50, 104654.

Joshi, A. S., Dincer, I., & Reddy, B. V. (2009). Thermodynamic assessment of photovoltaic systems. *Solar Energy*, 83(8), 1139–1149.

Kabir, E., Kumar, P., Kumar, S., Adelodun, A. A., & Kim, K. H. (2018). Solar energy: Potential and future prospects. *Renewable and Sustainable Energy Reviews*, 82, 894–900.

Kandeal, A. W., Algazzar, A. M., Elkadeem, M. R., Thakur, A. K., Abdelaziz, G. B., El-Said, E. M. S., … Fawzy, H. E. (2021). Nano-enhanced cooling techniques for photovoltaic panels: A systematic review and prospect recommendations. *Solar Energy*, 227, 259–272.

Kazem, H. A. (2019). Evaluation and analysis of water-based photovoltaic/thermal (PV/T) system. *Case Studies in Thermal Engineering*, 13, 100401.

Kazemian, A., Hosseinzadeh, M., Sardarabadi, M., & Passandideh-Fard, M. (2018a). Effect of glass cover and working fluid on the performance of photovoltaic thermal (PVT) system: An experimental study. *Solar Energy*, 173, 1002–1010.

Kazemian, A., Hosseinzadeh, M., Sardarabadi, M., & Passandideh-Fard, M. (2018b). Experimental study of using both ethylene glycol and phase change material as coolant in photovoltaic thermal systems

(PVT) from energy, exergy and entropy generation viewpoints. *Energy*, 162, 210–223.

Khare, V., Nema, S., & Baredar, P. (2016). Solar–wind hybrid renewable energy system: A review. *Renewable and Sustainable Energy Reviews*, 58, 23–33.

Kiani, M. R., Meshksar, M., Makarem, M. A., & Rahimpour, M. R. (2022). Preparation, stability, and characterization of nanofluids. In *Nanofluids and Mass Transfer* (pp. 21–38). Elsevier.

Ladjevardi, S. M., Asnaghi, A., Izadkhast, P. S., & Kashani, A. H. (2013). Applicability of graphite nanofluids in direct solar energy absorption. *Solar Energy*, 94, 327–334.

Lamb, W. F., Wiedmann, T., Pongratz, J., Andrew, R., Crippa, M., Olivier, J. G. J., … House, J. (2021). A review of trends and drivers of greenhouse gas emissions by sector from 1990 to 2018. *Environmental Research Letters*, 16(7), 73005.

Lee, J. H., Hwang, S. G., & Lee, G. H. (2019). Efficiency improvement of a photovoltaic thermal (PVT) system using nanofluids. *Energies*, 12(16), 3063.

Liu, J., Xue, Y., Zhang, M., & Dai, L. (2012). Graphene-based materials for energy applications. *MRS Bulletin*, 37(12), 1265–1272.

Mahdavi, S., Sarhaddi, F., & Hedayatizadeh, M. (2019). Energy/exergy based-evaluation of heating/cooling potential of PV/T and earth-air heat exchanger integration into a solar greenhouse. *Applied Thermal Engineering*, 149, 996–1007.

Makarieva, A. M., Gorshkov, V. G., & Li, B.-L. (2008). Energy budget of the biosphere and civilization: Rethinking environmental security of global renewable and non-renewable resources. *Ecological Complexity*, 5(4), 281–288.

Manikandan, E., Mayandi, K., Sivasubramanian, M., Rajini, N., Rajesh, S., Muthulakshmi, L., & Rashedi, A. (2022). A comprehensive review on the impact of nanofluid in solar photovoltaic/thermal system. *Proceedings of the Institution of Mechanical Engineers, Part C: Journal of Mechanical Engineering Science*, 236(9), 5078–5096.

Mbayachi, V. B., Ndayiragije, E., Sammani, T., Taj, S., & Mbuta, E. R. (2021). Graphene synthesis, characterization and its applications: A review. *Results in Chemistry*, 3, 100163.

Mehta, B., Subhedar, D., Panchal, H., & Said, Z. (2022). Synthesis, stability, thermophysical properties and heat transfer applications of nanofluid–A review. *Journal of Molecular Liquids*, 364, 120034.

Mustafa, R. J., Gomaa, M. R., Al-Dhaifallah, M., & Rezk, H. (2020). Environmental impacts on the performance of solar photovoltaic systems. *Sustainability*, 12(2), 608.

Oh, J., Bae, S., Chae, H., Jeong, J., & Nam, Y. (2023). Photovoltaic–thermal advanced technology for real applications: Review and case study. *Energy Reports*, 10, 1409–1433.

Pang, C., Lee, J. W., & Kang, Y. T. (2015). Review on

combined heat and mass transfer characteristics in nanofluids. *International Journal of Thermal Sciences*, 87, 49–67.

Pordanjani, A. H., Aghakhani, S., Afrand, M., Sharifpur, M., Meyer, J. P., Xu, H., … Cheraghian, G. (2021). Nanofluids: Physical phenomena, applications in thermal systems and the environment effects-a critical review. *Journal of Cleaner Production*, 320, 128573.

Prăvălie, R., Patriche, C., & Bandoc, G. (2019). Spatial assessment of solar energy potential at global scale. A geographical approach. *Journal of Cleaner Production*, 209, 692–721.

Rafaizul, N. I. A. M., Rosli, M. A. M., Salimen, N., Habibi, I. A., Permanasari, A. A., & Herawan, S. G. (2024). Applications of Graphene Nanoplatelets as Working Fluids in Photovoltaic Thermal Systems: A Review. *International Journal of Nanoelectronics and Materials (IJNeaM)*, 17(3), 343–353.

Rasheed, A. K., Khalid, M., Rashmi, W., Gupta, T., & Chan, A. (2016). Graphene based nanofluids and nanolubricants–Review of recent developments. *Renewable and Sustainable Energy Reviews*, 63, 346–362.

Sadeghinezhad, E., Mehrali, M., Saidur, R., Mehrali, M., Latibari, S. T., Akhiani, A. R., & Metselaar, H. S. C. (2016). A comprehensive review on graphene nanofluids: Recent research, development and applications. *Energy Conversion and Management*, 111,

466–487.

Safiei, W., Rahman, M. M., Yusoff, A. R., & Radin, M. R. (2020). Preparation, stability and wettability of nanofluid: A review. *Journal of Mechanical Engineering and Sciences*, 14(3), 7244–7257.

Saidur, R., Meng, T. C., Said, Z., Hasanuzzaman, M., & Kamyar, A. (2012). Evaluation of the effect of nanofluid-based absorbers on direct solar collector. *International Journal of Heat and Mass Transfer*, 55(21–22), 5899–5907.

Salameh, T., Tawalbeh, M., Juaidi, A., Abdallah, R., & Hamid, A.-K. (2021). A novel three-dimensional numerical model for PV/T water system in hot climate region. *Renewable Energy*, 164, 1320–1333.

Salari, A., Taheri, A., Farzanehnia, A., Passandideh-fard, M., & Sardarabadi, M. (2021). An updated review of the performance of nanofluid-based photovoltaic thermal systems from energy, exergy, economic, and environmental (4E) approaches. *Journal of Cleaner Production*, 282, 124318.

Salem Ahmed, M., Mohamed, A. S. A., & Maghrabie, H. M. (2019). Performance evaluation of combined photovoltaic thermal water cooling system for hot climate regions. *Journal of Solar Energy Engineering*, 141(4), 41010.

Sansaniwal, S. K., Sharma, V., & Mathur, J. (2018). Energy and exergy analyses of various typical solar energy applications: A comprehensive review. *Renewable and Sustainable Energy Reviews*, 82(May 2017), 1576–

1601.

Sardarabadi, M., Passandideh-Fard, M., & Heris, S. Z. (2014). Experimental investigation of the effects of silica/water nanofluid on PV/T (photovoltaic thermal units). *Energy*, 66, 264–272.

Shams, S. S., Zhang, R., & Zhu, J. (2015). Graphene synthesis: a review. *Materials Science-Poland*, 33(3), 566–578.

Sheikholeslami, M., Khalili, Z., & Mousavi, S. J. (2023). Influence of self-cleaning coating on performance of photovoltaic solar system utilizing mixture of phase change material and Graphene nanoparticle. *Journal of Building Engineering*, 77, 107540.

Shinohara, H., & Tiwari, A. (2015). *Graphene: an introduction to the fundamentals and industrial applications*. John Wiley & Sons.

Siow, L. T., Lee, J. R., Ooi, E. H., & Von Lau, E. (2024). Application of graphene and graphene derivatives in cooling of photovoltaic (PV) solar panels: A review. *Renewable and Sustainable Energy Reviews*, 193, 114288.

Souza, R. R., Gonçalves, I. M., Rodrigues, R. O., Minas, G., Miranda, J. M., Moreira, A. L. N., … Moita, A. S. (2022). Recent advances on the thermal properties and applications of nanofluids: From nanomedicine to renewable energies. *Applied Thermal Engineering*, 201, 117725.

Taheri, A., Kazemi, M., Amini, M., Sardarabadi, M., & Kianifar, A. (2021). The performance assessment of

nanofluid-based PVTs with and without transparent glass cover: outdoor experimental study with thermodynamics analysis. *Journal of Thermal Analysis and Calorimetry*, 143, 4025–4037.

Taylor, R., Coulombe, S., Otanicar, T., Phelan, P., Gunawan, A., Lv, W., … Tyagi, H. (2013). Small particles, big impacts: A review of the diverse applications of nanofluids. *Journal of Applied Physics*, 113(1).

Tembhare, S. P., Barai, D. P., & Bhanvase, B. A. (2022). Performance evaluation of nanofluids in solar thermal and solar photovoltaic systems: A comprehensive review. *Renewable and Sustainable Energy Reviews*, 153, 111738.

Timofeeva, E. V. (2011). Nanofluids for heat transfer–potential and engineering strategies. *Two Phase Flow, Phase Change and Numerical Modeling*, 435–450.

Trivedi, S., Lobo, K., & Matte, H. S. S. R. (2019). Synthesis, properties, and applications of graphene. In *Fundamentals and sensing applications of 2D materials* (pp. 25–90). Elsevier.

Vaka, M., Walvekar, R., Rasheed, A. K., Khalid, M., & Panchal, H. (2019). A review: emphasizing the nanofluids use in PV/T systems. *IEEE Access*, 8, 58227–58249.

Venkatesh, T., Manikandan, S., Selvam, C., & Harish, S. (2022). Performance enhancement of hybrid solar PV/T system with graphene based nanofluids. *International Communications in Heat and Mass Transfer*, 130, 105794.

Yandri, E. (2019). Development and experiment on the performance of polymeric hybrid Photovoltaic Thermal (PVT) collector with halogen solar simulator. *Solar Energy Materials and Solar Cells*, 201, 110066.

Yazdanifard, F., Ameri, M., & Ebrahimnia-Bajestan, E. (2017). Performance of nanofluid-based photovoltaic/thermal systems: A review. *Renewable and Sustainable Energy Reviews*, 76(December 2016), 323–352.

Zhao, B., Hu, M., Ao, X., Xuan, Q., & Pei, G. (2020). Spectrally selective approaches for passive cooling of solar cells: A review. *Applied Energy*, 262, 114548.

THEORETICAL AND EXPERIMENTAL APPROACHES IN SCIENTIFIC STUDIES

yaz
yayınları

YAZ Yayınları
M.İhtisas OSB Mah. 4A Cad. No:3/3
İscehisar / AFYONKARAHİSAR
Tel : (0 531) 880 92 99
yazyayinlari@gmail.com • www.yazyayinlari.com

ISBN: 978-625-6104-82-2